

# RENF: RETHINKING THE PRINCIPLES OF NEURAL LONG-TERM TIME SERIES FORECASTERS

Yihang Lu<sup>1,2</sup>, Xianwei Meng<sup>1</sup>, Enhong Chen<sup>2</sup>

<sup>1</sup>Hefei Institutes of Physical Science, Chinese Academy of Sciences, Hefei, China

<sup>2</sup>University of Science and Technology of China, Hefei, China

lyhsa22@mail.ustc.edu.cn

## ABSTRACT

Neural Forecasters (NFs) have become a cornerstone of Long-term Time Series Forecasting (LTSF). However, recent progress has been hampered by an overemphasis on architectural complexity at the expense of fundamental forecasting principles. In this work, we revisit the principles of LTSF. We begin by formulating a Variance Reduction Hypothesis (VRH), positing that generating and combining multiple forecasts is essential to reducing the inherent uncertainty of NFs. Guided by this, we propose Boosted Direct Output (BDO), a streamlined paradigm that synergistically hybridizes the causal structure of Auto-Regressive (AR) with the stability of Direct Output (DO), while implicitly realizing the principle of forecast combination within a single network. Furthermore, we address the critical validation-test generalization gap by employing parameter smoothing to stabilize optimization. Extensive experiments demonstrate that these trivial yet principled improvements enable a direct temporal MLP to outperform recent, complex state-of-the-art models in nearly all benchmarks, without relying on intricate inductive biases. Finally, we empirically verify our hypothesis, establishing a dynamic performance bound that highlights promising directions for future research. The code for review is available at: <https://anonymous.4open.science/r/ReNF-A151>.

## 1 INTRODUCTION

The progression of any real-world event is a unique, non-repeatable process, often governed by chaotic dynamics that we cannot perfectly measure (Robertson, 1929) or describe. This implies that any observed time series is a single stochastic realization of a complex underlying system, inevitably corrupted by measurement errors. Consequently, a fundamental open question persists: how can we best estimate long-term future states using a data-driven model that relies solely on a single observed historical sequence?

Deep Neural Networks (DNNs) have recently received considerable critical attention in Long-Term Time Series Forecasting (LTSF) (Kim et al., 2025). Their capacity to model high-dimensional, non-linear dependencies makes the Neural Forecaster (NF) a promising tool for capturing complex temporal dynamics (Laiz et al., 2024). However, the literature reveals several critical bottlenecks that have to be addressed to unlock the full potential of DNNs in this domain.

A confounding paradox in recent research is that advanced architectures, such as Transformer-based models (Nie et al., 2023), and simple linear models (Zeng et al., 2023) are reported to achieve state-of-the-art performance interchangeably, despite vast differences in complexity. This is partly because some datasets favor parsimonious models (Deng et al., 2024), while others possess sufficient volume to fit complex architectures. Yet, a deeper issue may be the insufficient exploration of the networks' intrinsic capabilities. As indicated by (Lu et al., 2025), many complex NFs contain redundant components that are activated selectively based on data properties, leaving their full potential untapped without extensive tuning.

Furthermore, the field has shifted towards designing specialized modules for specific properties, such as multi-scale modeling (Wang et al., 2024b) and non-stationarity adaptation (Liu et al., 2022). However, progress has become erratic, as these architectural additions often yield subtle gains while

overlooking fundamental principles. A primary and more general path to advancement may lie in fundamentally improving the training stability and generalization capabilities of NFs themselves.

Notably, training on time series often suffers from significant instability. The non-stationary nature of real-world time series, combined with chronological data splitting, leads to both internal (batch-to-batch) and external (train/validation/test) distribution mismatches. This causes the optimization path to be heterogeneous, rendering the learning process for NFs ineffective. Specifically, internal data redundancy can cause the model to overfit spurious patterns (Liu et al., 2025a), while external distribution shift creates inconsistencies across training phases. Although normalization techniques (Kim et al., 2021) address train-test shifts, a critical discrepancy remains between validation and testing performance, which insidiously prevents NFs from demonstrating their true capabilities.

Beyond model architecture, we identify a structural limitation in the dominant Direct Output (DO) framework: it fails to fully utilize available supervision. In a standard DO setup, an NF is trained as a single-input single-output system to predict the entire future horizon in a single forward pass, meaning the whole label information is leveraged only once per optimization step. This may tend to encourage the model to learn a monolithic structural representation that maps history directly to the future, without explicitly modeling the sequential dependencies within the forecast itself. We contend that this approach hinders the model from developing a more granular, causal understanding of the future, thereby limiting its full potential.

To address these fundamental issues, this paper proposes some principled improvements that help establish a reliable and high-performing NF. Our contributions are summarized as follows:

- We redesign the forecasting architecture with a novel, streamlined stacking paradigm that synergistically combines the causal structure of Auto-Regressive (AR) methods with the stability of Direct Output (DO).
- We identify the validation-test generalization gap as a critical bottleneck in evaluating Neural Forecasters. To bridge this gap, we adopt Exponential Moving Average (EMA), demonstrating that this standard technique is particularly effective in the LTSF domain for stabilizing optimization and preventing overfitting.
- We conduct extensive experiments to evaluate the effectiveness of our proposals and demonstrate that a pure MLP-based forecaster, when trained with our paradigm, can still outperform recent state-of-the-art models on nearly all standard LTSF benchmarks, establishing a new and efficient performance baseline for the field.

## 2 METHOD

In this section, we lay out the methodological foundations of our work. We begin by introducing a core hypothesis that provides the primary motivation for our multi-forecasts approach. To build intuition, we highlight the key effects of each consideration with empirical demonstrations using a toy MLP on selected datasets.

**Problem Formulation.** We define a Neural Forecasting Machine (NFM) as a mapping  $\Phi_\theta(X, \gamma) \rightarrow Y$ , where  $\theta$  denotes learnable parameters and  $\gamma$  represents the model’s stochastic state (e.g., random seeds). Given a dataset of finite realizations drawn from an underlying process, partitioned into history  $X_h \in \mathbb{R}^{T_x}$  and future  $X_f \in \mathbb{R}^{T_y}$ , the forecasting task aims to learn a NFM such that the generated prediction  $\hat{Y}_f = \Phi_\theta(X_h, \gamma)$  minimizes the error metric between  $\hat{Y}_f$  and  $X_f$ .

### 2.1 THEORETICAL MOTIVATION FOR MULTIPLE FORECASTS

We allow the trained NFM as a generator capable of producing *multiple outputs* for a fixed input, conditioned on varying internal states or configurations. To theoretically assess the capability of such a forecaster, we estimate the point-wise error between the generated predictions  $\hat{Y}_f$  and the expected future  $X_f$  as follows,

**Hypothesis 1** (Variance Reduction Hypothesis (VRH)). *Given a NFM  $\Phi_\theta$  and an observed time series  $X_h = (x_1, x_2, \dots, x_h)$  where each element  $x_t$  is drawn from the true distribution  $p_t(\mu_t, \sigma_t^2)$  with mean  $\mu$  and standard deviation  $\sigma_t$ . We hypothesis that one can generate a series from the forecasts*

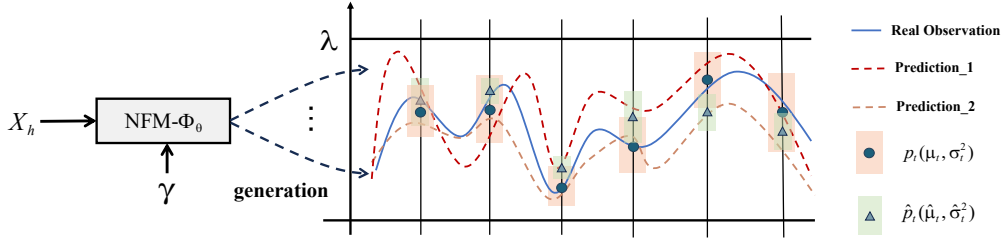


Figure 1: A single trained NFM  $\Phi_\theta$  can generate multiple forecasts from a fixed input  $X_h$  under various states  $\gamma$  and  $\theta$ . These forecasts are expected to follow the empirical process ( $\hat{p}_t, t = 1, 2, \dots$ ) approximated by the NFM with the observed data. The model-estimated process is distinguished from the real data distribution ( $p_t, t = 1, 2, \dots$ ) by a bias.

of  $\Phi$ :  $\hat{Y}_f = (y_1, y_2, \dots, y_N)$  with each element  $y_t$  drawn from the estimated future distribution  $\hat{p}(\hat{\mu}_t, \hat{\sigma}_t^2)$  such that the absolute error between  $\hat{Y}_f$  and  $X_f$  relates to a trivial upper bound,

$$\left( \underbrace{\sigma_t}_{\text{data variance}} + \underbrace{b}_{\text{predictive bias}} + \underbrace{\lambda/\sqrt{c}}_{\text{predictive variance}} \right) * N \quad (1)$$

where  $b := \sup_t |\hat{\mu}_t - \mu_t|$ ,  $\lambda$  can be the upper bound of the second moment of any single forecast, and  $c$  denotes the number of series.

**Remark.** This bound relies on independence assumptions, which simplifies the dependencies inherent in our empirical design. Nonetheless, the analysis provides a qualitative guide, exposing the problem of predictive variance and **motivating the shift from single-shot to multi-output forecasters.**

The detailed proof is provided in Appendix B.1. To interpret this bound value, we decompose the error into three distinct components. First,  $\sigma_t$  represents the intrinsic system uncertainty, which is irreducible by the model. Second, the predictive bias reflects the approximation gap between the learned and true distributions; while this can be reduced by enhancing model capacity, it has been the primary focus of prior research. Crucially, we argue that the final term, the predictive variance, is largely overlooked in the design of deterministic neural forecasters. By default, these models yield a single output ( $c = 1$ ), leaving this error component from the inherent uncertainty of a neural network unresolved. Unlike classical methods often constrained by closed-form derivations, NFs possess the intrinsic flexibility to generate multiple outputs, thereby actively reducing this variance.

**Post combination of multiple forecasts.** Given a set of candidate outputs from an NFM, there exist aggregation strategies to synthesize a single, integrated forecast that is more accurate than any individual candidate (Clemen, 1989). We represent this aggregation as a functional  $g_c$  that produces the post-combined forecast:

$$\hat{Y}_{pc} = g_c(\{\hat{Y}_f^{(i)}\}_{i=1}^c) \quad (2)$$

In Sec. 3.3, we empirically demonstrate that the performance of an 'oracle' combination on real-world datasets is consistent with the hypothesis. However, constructing an optimal combination in practice is non-trivial (Clemen, 1989) since intricate combination methods practically underperform the simple average (Stock & Watson, 2004). Consequently, a primary objective of our proposed framework is to bypass explicit combination design and instead enable the forecasting paradigm to *implicitly* learn itself how to leverage the information contained within these multiple forecasts.

## 2.2 NOVEL FORECASTING PARADIGM

The current frameworks in LTSF involve two main strategies: 1-step Auto Regressive (AR(1)) and Direct Output (DO). While AR models perform consistently with recurrent state space models like RNNs (Siarni-Namini et al., 2019), they are known to suffer from significant error accumulation in long-horizon forecasting and are empirically evidenced to largely fall behind DO in LTSF (Zhou et al., 2021), making a strong reason for the dominant position of DO in LTSF. However, the shortcomings of the DO approach itself have been largely overlooked. We argue that

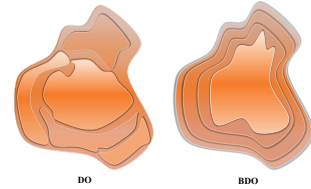


Figure 2: Features of DO and BDO.

However, the shortcomings of the DO approach itself have been largely overlooked. We argue that

despite its simplicity, the most significant weakness of DO, particularly when compared to AR, is its lack of inherent causality in the structure of the predictive representations.

To illustrate this, we conduct a simple experiment in Fig.3: we consecutively split a forecast of length  $L$  into  $m$  non-overlapped chunks with length  $L/m$ , and each is predicted by an independent linear head from a shared representation. The final forecast is a concatenation of these segments. Empirically, it turns out that the performance of this multi-headed model is nearly identical to a standard DO model with a single head predicting the full horizon. This result suggests that the NF is almost unaware of the temporal relationships within the future sequence and makes the prediction without considering the interval between the input history and the output future. As a result, it learns to forecast each segment independently, which seems anti-intuitive.

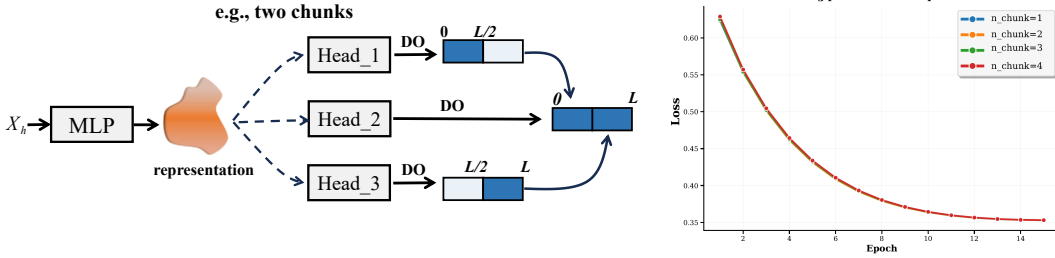


Figure 3: We make the forecast by applying independent heads on several non-overlapped chunks. The right figure shows the training loss curve in different settings.

According to this observation, and combining our heuristic idea from VRH, we propose a new forecasting paradigm as follows,

**Definition 1** (Boosted Direct Output (BDO)). *Given a history time series  $X = \{x_1, x_2, \dots, x_h\}$  (abbr.  $X\{1:h\}$ ) with length  $h$ , the NF recursively generates the forecast  $\hat{Y}$  of the future object  $Y = \{y_1, y_2, \dots, y_L\}$  over  $N$ -steps. Let  $\hat{Y}\{1:h_{n-1}\}$  be the forecast at step  $n-1$ , then the forecast at step  $n$  is:*

$$\hat{Y}\{1:h_n\} = NF([X, \hat{Y}\{1:h_{n-1}\}]), \quad n = 1, 2, \dots, N; \quad (3)$$

where  $h_0 = 1$  and  $h_N = y_L$ .  $[\cdot, \cdot]$  indicates the concatenation along the temporal dimension,  $L$  is the entire prediction length. In our implementation, we evenly split the forecasting length into  $n$  segments for convenience, i.e., in Eq. 3,  $h_N = h * N$ , where  $N$  is a factor of  $L$ .

**Remark.** *BDO generalizes DO but is distinct from AR. Unlike existing AR paradigms (Salinas et al., 2020) which feed predictions back to yield the next step consecutively, BDO regenerates the horizon from the start point at each iteration. Thus, every intermediate output is a complete, independent sub-forecast rather than a dependent fragment of a single trajectory.*

Intuitively, BDO recursively generates forecasts for progressively longer horizons, reusing predictions from previous stages. This incorporates an AR-like causal structure into the forecasting process, while retaining the patch-wise output characteristic of DO that mitigates significant error accumulation. A balance between these two properties can be achieved by properly setting the number of recursive stages,  $N$  (see Appendix B.1 for theoretical analysis). Furthermore, since short-term forecasting is generally an easier task than long-term forecasting, BDO effectively creates a learning curriculum and tends to build hierarchical representations as illustrated in Fig.2. We can reasonably expect this paradigm to outperform both pure AR and pure DO strategies, especially in the challenging LTSF setting.

### 2.3 MODEL ARCHITECTURE

We construct our NFs using only MLP and linear layers for: 1) As foundational deep learning modules, improvements demonstrated on them are broadly applicable and convincing. 2) Recent work has shown that MLP-based architectures perform well for a wide range of forecasting tasks (Ekambaram et al., 2023).

Fundamentally, we build two NF variants, ReNF- $\alpha$  and ReNF- $\beta$ , which differ in their degree of non-linearity for handling datasets of varying complexity. The overall architecture is shown in Fig.4, which is characterized by two main principles.

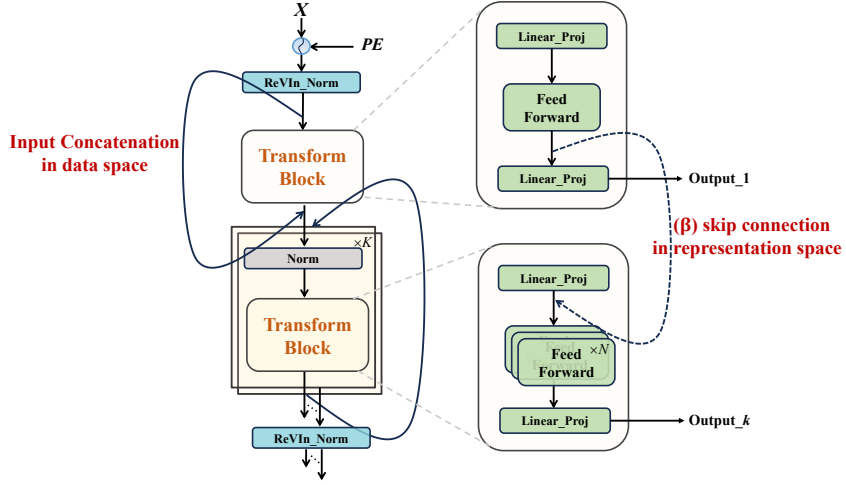


Figure 4: Model Structure of ReNF. PE denotes optional embeddings, and the  $\beta$  version adds additional skip-connections for deeper representations.

**Block-wise Supervision.** To adopt the BDO strategy, we stack multiple blocks, and each consists of a linear layer for representation projection, followed by an MLP for nonlinear transformation. Particularly, the end of each block is equipped with a dedicated linear head that maps the internal representation back to the data space, steering it to function as a **sub-forecaster** for horizon  $h_j$ .

**Generalized Forecast Combination.** In the recursive BDO process, each sub-forecast is concatenated with the original input to form the new input for the next block. This operation is trivial yet crucial in our design as it allows an implicit generalized forecast combination as follows,

$$\hat{Y}\{1:h_n\} = \text{NF}([X, \hat{Y}\{1:h_{n-1}\}]) = \begin{bmatrix} \underbrace{X}_{\text{Input}} & \underbrace{\hat{Y}\{1:h_{n-1}\}}_{\text{Last Forecast}} \end{bmatrix} \cdot \begin{bmatrix} f \\ \varphi \end{bmatrix} = f(X) + \varphi(\hat{Y}) \quad (4)$$

where we characterize the  $n$ -th MLP block as an operator composed by  $f: \mathbb{R}^h \rightarrow \mathbb{R}^{h_n}$  and  $\varphi: \mathbb{R}^{h_{n-1}} \rightarrow \mathbb{R}^{h_n}$ . Thus, if we densely connect all outputs, every intermediate stage of the NF will recursively learn the implicit combination and finally yield a complex composed forecast.

We employ RevIN (Kim et al., 2021) as the pre-normalization for the initial input data to reduce the distribution discrepancy between the training and evaluation phases. For consistency, we also apply pre-normalizations to the input of each sub-forecaster. Additionally, we apply dropout before the initial linear projection to prevent the model from being overly dependent on the history observation and the concatenated information in the data space. To allow for representation flow with diverse depths, the ReNF- $\beta$  variant also incorporates skip-connections between the representation spaces.

The general equation for the transformation process within each sub-forecaster can be written as follows,

$$\text{ReNF\_Block}(T) = \text{Proj}(\text{Transform}(\text{Proj}(\text{Norm}(\text{Drop}(T)))))) \quad (5)$$

where  $T$  denotes the input series, and all the projections are performed on the temporal dimension.

## 2.4 LEARNING OBJECTIVE

To train a deterministic NF, we adopt the hybrid loss function as used in (Liu et al., 2025a), which is a convex combination of the Mean Absolute Error (MAE) in both the time and frequency domains. The frequency-domain component has been shown to be effective at reducing spurious autocorrelations in the labels (Wang et al., 2024a).

Our BDO framework uniquely generates multiple outputs of varying lengths, enabling us to apply this loss at each forecasting stage. This hierarchical supervision allows us to fully leverage the label information at multiple scales, encouraging the model to build causally structured and homogeneous representations rather than the disconnected ones typical of standard DO forecasts.

To ensure a stable foundation as well as the diversity of different forecasts, we place heavier weights on the losses of earlier short-term sub-forecasts. The complete loss function is expressed as follows:

$$loss = \sum_{n=1}^N (\gamma/n) * (\alpha * \|\hat{Y}_f^{(n)} - X_f^{(n)}\|_1 + (1 - \alpha) * \|\text{Freq}(\hat{Y}_f^{(n)}) - \text{Freq}(X_f^{(n)})\|_1) \quad (6)$$

where  $\|\cdot\|_1$  denotes the  $l_1$  norm,  $\gamma$  and  $\alpha$  is predefined coefficients.  $\text{Freq}(\cdot)$  represents the discrete fourier transform and  $\hat{Y}_f^{(n)}$  denotes the  $n$ -th sub-forecast corresponding to the  $n$ -th block of the model. A more in-depth analysis of this loss function is provided in Appendix C.

### 2.5 SMOOTHING THE LEARNING FOR TIME SERIES

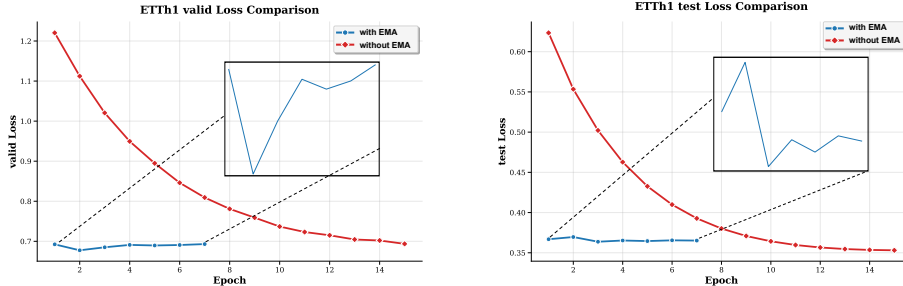


Figure 5: Variation of valid and test loss with and without applying EMA weight averaging. The valid loss and test loss are not consistent during the learning process of NFs without smoothing.

On many time series datasets, particularly those with smaller volumes, the validation and test losses exhibit significantly different and, at times, conflicting dynamics during training. This issue invalidates the early stopping criterion: learning steps become ineffective, and suboptimal models are saved, preventing a true assessment of a model’s capabilities. This is especially problematic when comparing models of varying complexities, which naturally have different optimization trajectories.

To mitigate these unexpected effects, we propose smoothing the training trajectory by employing an averaged model for evaluation. We achieve this efficiently using an Exponential Moving Average (EMA) to track the parameters of the online model (Izmailov et al., 2018). While this has been a standard technique in self-supervised learning (He et al., 2020) and generative modeling (Song et al., 2020), its critical role in mitigating the specific distribution shifts found in LTSF has been largely underexplored. We empirically establish it as a necessary protocol for robust performance. Specifically, let  $\theta$  be the parameters of the online model being trained, and  $\theta'$  be the parameters of the shadow model. Then the shadow model’s parameters are upgraded as follows at each iteration.

$$\theta'_{new} = \alpha * \theta'_{prev} + (1 - \alpha) * \theta_{current} \quad (7)$$

where  $\alpha$  is the EMA decay rate. This shadow model is then used for all evaluations. As shown in Fig. 5, this technique effectively smooths the learning curves and mitigates the inconsistency between validation and test performance. By providing a more stable and reliable training signal, EMA prolongs the effective learning period and allows the model to converge to better local minima, achieving improved generalization.

## 3 EXPERIMENT

**Baselines and Datasets.** Our empirical evaluation is designed to first establish the core strengths of our method in its intended domain and then to verify its generality across a wider range of forecasting tasks. Accordingly, the main text concentrates on established multivariate long-term forecasting benchmarks (ETTh, Electricity, Weather, etc.), where the hierarchical, variance-mitigating structure of BDO is particularly effective. To validate the versatility of our approach, we then present a comprehensive suite of supplementary experiments in the Appendix. These evaluations test our proposals on distinct domains, including diverse short-term forecasting from Kaggle (Yue et al., 2025), spatio-temporal traffic data (PEMS), and classical univariate series (M4 competition (Wang et al., 2024b)). A complete description of these datasets can be found in Appendix A.

For the multivariate long-term forecasting, we compare our model with a suite of recent state-of-the-art methods, including TimeBridge (Liu et al., 2025a), DUET (Qiu et al., 2025), TimeDistill (Ni et al., 2025), Timer-XL (Liu et al., 2025b), iTransformer (Liu et al., 2024), TimeMixer (Wang et al., 2024b), PatchTST (Nie et al., 2023), Crossformer (Zhang & Yan, 2023), and Dlinear (Zeng et al., 2023).

**Setups.** All experiments were conducted on a single NVIDIA 4090 GPU with 24GB of memory, using the Adam optimizer (Kingma & Ba, 2014) and a fixed random seed of 2021 for reproducibility. Results for all baseline models were reproduced using their official source code and optimal configurations. For our model, ReNF, we searched for the optimal learning rate in the range from 0.0001 to 0.005, the EMA decay rates in the range from 0.99 to 0.999, and the number of layers from 2 to 8. We apply ReNF- $\alpha$  to ETTh1 and ETTh2 datasets, and ReNF- $\beta$  to others. The look-back window of all models is searched over {336, 512, 720} for the best long-term forecasting performance following the standard benchmark configuration (Qiu et al., 2025).

### 3.1 MAIN RESULT

The results, presented in Table 2, demonstrate a critical finding: a well-executed, straight-forward MLP-based architecture can still outperform complex state-of-the-art models. Notably, we achieve these gains without relying on intricate mechanisms such as multi-resolution and periodicity. By focusing instead on fundamentally improving the forecasting principles, our MLP model-ReNF sets a new state-of-the-art. Overall, ReNF surpasses all leading 2024 models by a significant margin and outperforms even the very competitive 2025 SOTA methods in almost all cases. This manifestation of contrast provides strong evidence for the effectiveness of our proposed techniques.

However, we do not claim that existing specialized techniques are redundant. Rather, as discussed in Sec.2.5, many of these architectural designs were evaluated within unstable training frameworks, suggesting that their true effects may need tedious re-evaluation, which may be a promising future work. For instance, on the Traffic dataset, while ReNF shows significant improvement over many baselines, it does not surpass the MSE score of the large Transformer-based model, TimeBridge. We compare the model complexity between the most competitive models in the Table 1, showing that ReNF reduces 20x the complexity in FLOPs compared to TimeBridge with the Traffic dataset. This suggests that more complex models might still work better on datasets with high volume.

Model		ReNF	TimeBridge	DUET
Weather	Params (MB)	<b>0.200</b>	0.887	4.128
	FLOPs (GB)	<b>0.004</b>	4.262	0.143
ETTh2	Params (MB)	<b>0.393</b>	0.460	4.658
	FLOPs (GB)	<b>0.003</b>	1.604	0.051
Traffic	Param (MB)	21.476	12.431	<b>9.910</b>
	FLOPs (GB)	22.813	479.231	<b>15.575</b>

Table 1: Efficiency comparison of ReNF, TimeBridge, and DUET. All metrics are averaged across the four prediction lengths.

Models	ReNF ours		TimeBridge ((2025a))		DUET ((2025))		TimeDistill ((2025))		Timer-XL ((2025b))		iTransformer ((2024))		TimeMixer ((2024b))		PatchTST ((2023))		Crossformer ((2023))		DLinear ((2023))	
	MSE	MAE	MSE	MAE	MSE	MAE	MSE	MAE	MSE	MAE	MSE	MAE	MSE	MAE	MSE	MAE	MSE	MAE	MSE	MAE
Weather	<b>0.214</b>	<b>0.247</b>	0.220	<b>0.250</b>	<b>0.219</b>	0.253	0.221	0.269	0.240	0.273	0.232	0.269	0.226	0.264	0.224	0.262	0.232	0.294	0.242	0.293
Electricity	<b>0.145</b>	<b>0.237</b>	<b>0.152</b>	<b>0.247</b>	0.157	0.248	0.157	0.254	0.155	0.246	0.163	0.258	0.185	0.284	0.171	0.271	0.171	0.263	0.167	0.264
Traffic	<b>0.365</b>	<b>0.245</b>	<b>0.357</b>	<b>0.248</b>	0.393	0.256	0.387	0.271	0.374	0.255	0.395	0.279	0.409	0.279	0.397	0.275	0.522	0.282	0.418	0.287
Solar	<b>0.176</b>	<b>0.214</b>	<b>0.183</b>	0.219	0.195	<b>0.214</b>	0.184	0.242	0.198	0.249	0.202	0.262	0.193	0.252	0.200	0.284	0.205	0.233	0.224	0.286
ETTh1	<b>0.331</b>	<b>0.364</b>	0.349	0.380	<b>0.338</b>	<b>0.369</b>	0.348	0.380	0.359	0.382	0.361	0.390	0.356	0.380	0.349	0.381	0.464	0.456	0.356	0.379
ETTh2	<b>0.243</b>	<b>0.301</b>	<b>0.247</b>	<b>0.305</b>	0.248	0.308	0.250	0.312	0.271	0.322	0.269	0.327	0.257	0.318	0.256	0.314	0.501	0.505	0.259	0.325
ETTh1	<b>0.391</b>	<b>0.416</b>	<b>0.401</b>	0.426	0.401	<b>0.420</b>	0.430	0.441	0.409	0.430	0.439	0.448	0.427	0.441	0.419	0.436	0.439	0.461	0.425	0.439
ETTh2	<b>0.327</b>	<b>0.379</b>	0.345	0.386	<b>0.336</b>	<b>0.385</b>	0.345	0.395	0.352	0.402	0.370	0.403	0.349	0.397	0.351	0.395	0.894	0.680	0.470	0.468

Table 2: Results of long-term forecasting of hyperparameter searching. All results are averaged across four different prediction lengths: {96, 192, 336, 720}. The best and second-best results are highlighted in red and blue, respectively. Full results are listed in Appendix D.

### 3.2 ABLATION STUDY

**Effect of EMA.** To analyze the impact of EMA, we recorded the evaluation dynamics of ReNF with and without our smoothing technique. The results, shown in Fig. 6, clearly demonstrate EMA’s role. It is notable that we also record the variation of test loss as evidence for the effect of improving the generalization ability.

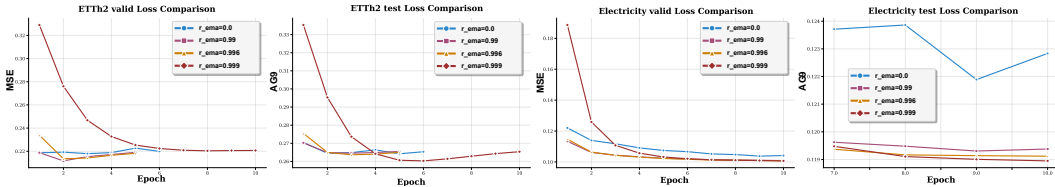


Figure 6: Effect of the EMA smoothing on training and test phase.

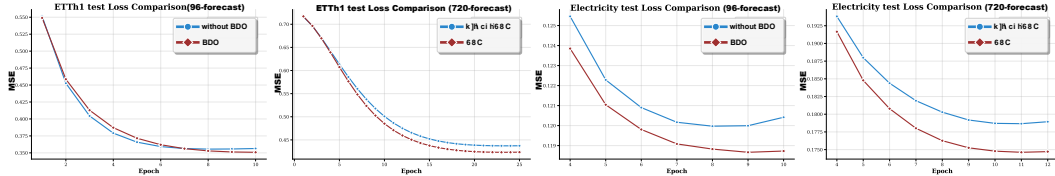


Figure 7: Effect of the BDO forecast.

First, on smaller or less stable datasets like ETTh2, EMA mitigates spurious overfitting and stabilizes the learning curves. This provides a more reliable signal for early stopping and prolongs the effective training period. Second, on large, high-quality datasets such as Electricity, the choice of EMA decay rate can influence performance. By selecting an appropriate rate, the generalization ability of the NF can be substantially enhanced. Full numerical results for all datasets are available in the Appendix E.3. These results show clearly the advantages of leveraging the model weight averaging technique and strongly support our claim in addressing the issue of valid-test inconsistency when training a neural forecaster for time series.

**Effect of BDO.** We investigate the effect of the BDO paradigm with the following settings: 1) Keep the depth of ReNF, but disable the recursive input concatenation and apply the loss function only to the final output; 2) Directly change the number of layers/sub-forecasts. By config.1, the BDO reduces to DO with the model structure unchanged. The results, shown in Fig. 7, demonstrate that even on the ETTh1 dataset, which has limited data and is difficult to optimize with deep representations, our BDO strategy can still yield superior performance, especially for very long-term forecasts. This finding empirically supports our claim, derived from proposition 2.1, that leveraging multiple, hierarchically-generated sub-forecasts provides valuable mutual information that enhances the final prediction.

Layer		K=1	K=2	K=3	K=4	K=5	K=6
Weather	MSE	0.311	0.309	0.307	0.307	0.307	0.307
	MAE	0.322	0.320	0.319	0.319	0.319	0.319
ETTh1	MSE	0.411	0.408	0.407	0.406	0.404	0.401
	MAE	0.411	0.409	0.408	0.407	0.407	0.407
Traffic	MSE	0.426	0.415	0.410	0.406	0.403	0.402
	MAE	0.281	0.274	0.272	0.270	0.267	0.267

Table 3: 720-length forecast with varying number of layers (sub-forecasts).

Furthermore, it is shown clearly in Fig. 8(a) that the performance of ReNF with the BDO strategy can consistently improve as  $K$  increases. In stark contrast, the performance of the DO model stagnates or degrades with added depth. This difference highlights BDO’s ability to effectively utilize deeper architectures. This meaningful phenomenon suggests that our paradigm may unlock a new, more effective scaling potential for NFs. Diverse examples are shown in the Table 3 and the Appendix D.

### 3.3 EMPIRICAL EVALUATION OF THE HYPOTHESIS

Dataset		ETTh1	ETTh2	Weather	Electricity	Solar	Traffic		
ReNF	Last Forecast	0.331	0.243	0.391	0.327	0.214	0.145	0.176	0.365
	Empirical Bound	0.225	0.201	0.270	0.252	0.165	0.100	0.090	0.254

Table 4: Comparison between the last single forecast and the optimal post-combined forecast of ReNF. The shown metrics are MSE and are averaged across the four prediction lengths.

To empirically evaluate our variance reduction hypothesis, we implement the post-combination strategy described in Sec. 2.1. This requires a combination functional,  $g_c$ . While finding an optimal

solution in practice is difficult, we can establish a theoretical upper bound on performance for the use of evaluation. Given the ground truth labels, a trivial yet optimal strategy is to select, at each timestep, the forecast value from among all candidates that has the smallest error. By applying this "oracle" combination, we aim to explore two points: 1) to quantify the potential accuracy improvement achievable through post-combination, thereby establishing a dynamic empirical bound for our forecasting model; and 2) to verify that this empirical bound behaves in a manner consistent with the intuitions of the VRH 2.1.

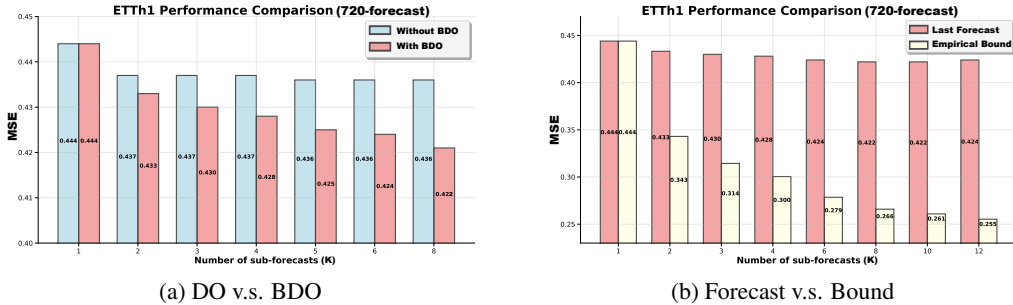


Figure 8: Performance variation with different numbers of sub-forecasts  $K$ . (a). Comparison of using DO or BDO. (b). Comparison between the best forecast and the empirical bound of ReNF.

Table 4 presents the performance of this oracle post-combination strategy, revealing a significant gap between the final ReNF forecast and the empirically optimal combination. While this oracle performance is unattainable in practice, the resulting empirical bound is highly informative. On one hand, it indicates that any single forecast is suboptimal and that powerful combinatorial strategies for improving predictions must exist (a promising direction for future work). On the other hand, it shows that we are still far from perfectly leveraging the information contained within the multiple sub-forecasts. This gap is precisely what motivates our BDO paradigm, which is designed to help the neural network implicitly learn a more effective combination function  $g_c$ .

Furthermore, Fig. 8(b) shows how this empirical bound varies with the number of sub-forecasts  $K$ . The bound consistently decays as  $K$  increases, even when the model’s performance saturates. This result aligns perfectly with the core insight from VRH: the theoretical performance limit improves as the number of candidate forecasts grows.

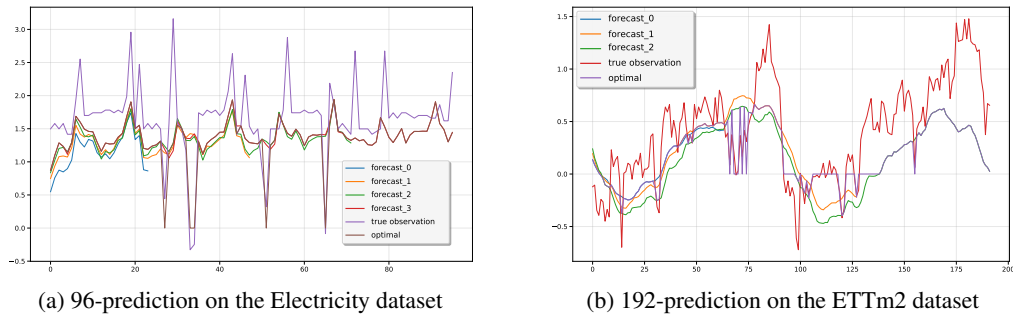


Figure 9: Visualization of forecasting results of ReNF. The figure shows multiple outputs of ReNF in different layers, along with the result of applying optimal post-combination.

In a nutshell, our evaluation of the VRH clarifies two primary roles for Neural Networks in this domain. First, NNs should be leveraged to learn a powerful post-combination function over multiple candidate forecasts. Second, more powerful base forecasters must be developed to better approximate the true data-generating distribution, directly reducing the predictive bias  $b$  as identified in our proposition 2.1.

## 4 RELATED WORK

**Ensemble.** Our work connects to classic ensemble methods in machine learning (Mohri et al., 2018). For instance, the recursive workflow of ReNF is analogous to gradient-boosted regression models (Chen & Guestrin, 2016), which construct a strong predictor from multiple weak ones. Additionally, the collaborative training can be viewed as a form of bagging (Breiman, 1996), which effectively resamples the data to train diverse forecasters. In this context, an even more recent study (Modi & Pan, 2025) re-certified the benefits of such ensemble methods for enhancing Transformer-based NFs, providing further empirical support for the direction of our research.

Forecast combination is a classic ensemble technique for improving forecast accuracy and robustness by leveraging the diverse strengths of multiple models (Clemen, 1989). In this work, we revisit this concept (Bates & Granger, 1969) in the domain of deep learning for long-term time series forecasting. Rather than combining distinct, parallel forecasters into a hybrid model (Zhang, 2003), our framework achieves this goal efficiently within a single, structured approach for generating and implicitly combining forecasts within a single neural network.

Our approach shares a conceptual lineage with deep stacking architectures (Wolpert, 1992) like N-BEATS (Oreshkin et al., 2019) and N-HiTS (Challu et al., 2023), which also synthesize a final forecast from multiple sub-modules. However, the fundamental motivation and aggregation mechanism differ. While N-BEATS and N-HiTS rely on additive residual decomposition—where subsequent blocks focus on correcting the errors (or specific frequency components) of previous blocks—our BDO paradigm employs recursive input concatenation. Instead of summing independent components, ReNF generates forecasts in a curriculum-style progression (from short-term to long-term horizons). By explicitly feeding earlier sub-forecasts back into the input space of subsequent layers, ReNF enforces a sequential dependency and allows the model to iteratively refine its understanding of the temporal trajectory, rather than performing a static multi-scale decomposition.

A recently proposed work using the multiple-choice learning paradigm (Cortés et al., 2025) is also relevant, as it demonstrates an ability to handle the diverse and multi-modal nature of the future from a probabilistic perspective. Furthermore, the characterization of TimeMCL as a conditional stationary quantizer for time series may offer additional theoretical support and interpretations for our framework.

**Short to Long Forecasting.** We note that ReNF is not the first work to address LTSF using multiple short-term forecasts. A pioneering and highly relevant study by (Nguyen & Chan, 2004) proposed a machine called MNN, which generates long-term forecasts using multiple neural networks, each responsible for a specific interval of the output. The essential distinction between MNN and our approach is that we generate sub-forecasts recursively, with the explicit goal of injecting causality into the DO strategy. In contrast, each sub-network in MNN functions as a standalone AR(1) model. This difference stems from our distinct motivation: whereas MNN was designed primarily to mitigate the error accumulation of one-step-ahead NN models, our work begins with a foundational forecasting proposition. Based on this proposition, we leverage modern deep learning techniques to effectively utilize multiple sub-forecasts, achieving strong empirical results on a wide range of real-world datasets, which constitutes one of our main contributions.

## 5 CONCLUSION

We locate some fundamental issues in the current design of neural forecasters. By proposing a Variance Reduction Hypothesis, we introduce a novel forecasting paradigm that combines the advantages of current forecasting methods and the principle of forecast combination, enabling more accurate predictions in a hierarchical structured representation space. We identify the weight averaging technique (e.g., EMA) as a critical, yet often overlooked, component for resolving the validation-test discrepancy in neural forecasting, serving to smooth the volatile learning process inherent to time series data. Our empirical results show that with these techniques, a simple MLP can still outperform recent SOTA models. The value of our hypothesis is also evaluated and confirmed by experimental results, clearly identifying the role of the Neural Network in building the Long-Term Time Series forecasters.

## 6 REPRODUCIBILITY STATEMENT

We have put a lot of effort into ensuring the reproducibility of this work, including the code in the anonymous repository <https://anonymous.4open.science/r/ReNF-A151>, a complete data description in the Appendix A, and clear explanations of the assumptions and proof of the proposition in the Appendix B.1.

## REFERENCES

- John M Bates and Clive WJ Granger. The combination of forecasts. *Journal of the operational research society*, 20(4):451–468, 1969.
- Leo Breiman. Bagging predictors. *Machine learning*, 24(2):123–140, 1996.
- Cristian Challu, Kin G. Olivares, Boris N. Oreshkin, Federico Garza Ramirez, Max Mergenthaler-Canseco, and Artur Dubrawski. Nhits: neural hierarchical interpolation for time series forecasting. 2023. doi: 10.1609/aaai.v37i6.25854. URL <https://doi.org/10.1609/aaai.v37i6.25854>.
- Tianqi Chen and Carlos Guestrin. Xgboost: A scalable tree boosting system. In *Proceedings of the 22nd acm sigkdd international conference on knowledge discovery and data mining*, pp. 785–794, 2016.
- Robert T Clemen. Combining forecasts: A review and annotated bibliography. *International journal of forecasting*, 5(4):559–583, 1989.
- Adrien Cortés, Rémi Rehm, and Victor Letzelter. Winner-takes-all for multivariate probabilistic time series forecasting. *arXiv preprint arXiv:2506.05515*, 2025.
- Jinliang Deng, Feiyang Ye, Du Yin, Xuan Song, Ivor Tsang, and Hui Xiong. Parsimony or capability? decomposition delivers both in long-term time series forecasting. *Advances in Neural Information Processing Systems*, 37:66687–66712, 2024.
- Vijay Ekambaram, Arindam Jati, Nam Nguyen, Phanwadee Sinthong, and Jayant Kalagnanam. Tsmixer: Lightweight mlp-mixer model for multivariate time series forecasting. In *Proceedings of the 29th ACM SIGKDD conference on knowledge discovery and data mining*, pp. 459–469, 2023.
- Kaiming He, Haoqi Fan, Yuxin Wu, Saining Xie, and Ross Girshick. Momentum contrast for unsupervised visual representation learning. In *Proceedings of the IEEE/CVF conference on computer vision and pattern recognition*, pp. 9729–9738, 2020.
- P Izmailov, AG Wilson, D Podoprikin, D Vetrov, and T Garipov. Averaging weights leads to wider optima and better generalization. In *34th Conference on Uncertainty in Artificial Intelligence 2018, UAI 2018*, pp. 876–885, 2018.
- Jongseon Kim, Hyungjoon Kim, HyunGi Kim, Dongjun Lee, and Sungroh Yoon. A comprehensive survey of deep learning for time series forecasting: architectural diversity and open challenges. *Artificial Intelligence Review*, 58(7):1–95, 2025.
- Taesung Kim, Jinhee Kim, Yunwon Tae, Cheonbok Park, Jang-Ho Choi, and Jaegul Choo. Reversible instance normalization for accurate time-series forecasting against distribution shift. In *International conference on learning representations*, 2021.
- Diederik P Kingma and Jimmy Ba. Adam: A method for stochastic optimization. *arXiv preprint arXiv:1412.6980*, 2014.
- Dilfira Kudrat, Zongxia Xie, Yanru Sun, Tianyu Jia, and Qinghua Hu. Patch-wise structural loss for time series forecasting. *arXiv preprint arXiv:2503.00877*, 2025.
- Rodrigo González Laiz, Tobias Schmidt, and Steffen Schneider. Self-supervised contrastive learning performs non-linear system identification. *arXiv preprint arXiv:2410.14673*, 2024.

- Peiyuan Liu, Beiliang Wu, Yifan Hu, Naiqi Li, Tao Dai, Jigang Bao, and Shu-tao Xia. Timebridge: Non-stationarity matters for long-term time series forecasting. *arXiv preprint arXiv:2410.04442*, 2025a.
- Yong Liu, Haixu Wu, Jianmin Wang, and Mingsheng Long. Non-stationary transformers: Exploring the stationarity in time series forecasting. *Advances in neural information processing systems*, 35: 9881–9893, 2022.
- Yong Liu, Tengge Hu, Haoran Zhang, Haixu Wu, Shiyu Wang, Lintao Ma, and Mingsheng Long. itransformer: Inverted transformers are effective for time series forecasting. *arXiv preprint arXiv:2310.06625*, 2024.
- Yong Liu, Guo Qin, Xiangdong Huang, Jianmin Wang, and Mingsheng Long. Timer-xl: Long-context transformers for unified time series forecasting. *arXiv preprint arXiv:2410.04803*, 2025b.
- Yihang Lu, Yangyang Xu, Qitao Qin, and Xianwei Meng. Timecapsule: Solving the jigsaw puzzle of long-term time series forecasting with compressed predictive representations. In *Proceedings of the 31st ACM SIGKDD Conference on Knowledge Discovery and Data Mining V. 2*, pp. 1987–1998, 2025.
- Dhruv D Modi and Rong Pan. Enhancing transformer-based foundation models for time series forecasting via bagging, boosting and statistical ensembles. *arXiv preprint arXiv:2508.16641*, 2025.
- Mehryar Mohri, Afshin Rostamizadeh, and Ameet Talwalkar. *Foundations of machine learning*. MIT press, 2018.
- Hanh H Nguyen and Christine W Chan. Multiple neural networks for a long term time series forecast. *Neural Computing & Applications*, 13(1):90–98, 2004.
- Juntong Ni, Zewen Liu, Shiyu Wang, Ming Jin, and Wei Jin. Timedistill: Efficient long-term time series forecasting with mlp via cross-architecture distillation. *arXiv preprint arXiv:2502.15016*, 2025.
- Yuqi Nie, Nam H Nguyen, Phanwadee Sinthong, and Jayant Kalagnanam. A time series is worth 64 words: Long-term forecasting with transformers. *arXiv preprint arXiv:2211.14730*, 2023.
- Boris N Oreshkin, Dmitri Carpov, Nicolas Chapados, and Yoshua Bengio. N-beats: Neural basis expansion analysis for interpretable time series forecasting. *arXiv preprint arXiv:1905.10437*, 2019.
- Xihao Piao, Zheng Chen, Taichi Murayama, Yasuko Matsubara, and Yasushi Sakurai. Fredformer: Frequency debiased transformer for time series forecasting. In *Proceedings of the 30th ACM SIGKDD conference on knowledge discovery and data mining*, pp. 2400–2410, 2024.
- Xiangfei Qiu, Xingjian Wu, Yan Lin, Chenjuan Guo, Jilin Hu, and Bin Yang. Duet: Dual clustering enhanced multivariate time series forecasting. In *Proceedings of the 31st ACM SIGKDD Conference on Knowledge Discovery and Data Mining V. 1*, pp. 1185–1196, 2025.
- Howard Percy Robertson. The uncertainty principle. *Physical Review*, 34(1):163, 1929.
- David Salinas, Valentin Flunkert, Jan Gasthaus, and Tim Januschowski. Deepar: Probabilistic forecasting with autoregressive recurrent networks. *International journal of forecasting*, 36(3): 1181–1191, 2020.
- Sima Siami-Namini, Neda Tavakoli, and Akbar Siami Namin. The performance of lstm and bilstm in forecasting time series. In *2019 IEEE International conference on big data (Big Data)*, pp. 3285–3292. IEEE, 2019.
- Yang Song, Jascha Sohl-Dickstein, Diederik P Kingma, Abhishek Kumar, Stefano Ermon, and Ben Poole. Score-based generative modeling through stochastic differential equations. *arXiv preprint arXiv:2011.13456*, 2020.

- James H Stock and Mark W Watson. Combination forecasts of output growth in a seven-country data set. *Journal of forecasting*, 23(6):405–430, 2004.
- Hao Wang, Licheng Pan, Zhichao Chen, Degui Yang, Sen Zhang, Yifei Yang, Xinggao Liu, Haoxuan Li, and Dacheng Tao. Fredf: Learning to forecast in the frequency domain. *arXiv preprint arXiv:2402.02399*, 2024a.
- Shiyu Wang, Haixu Wu, Xiaoming Shi, Tengge Hu, Huakun Luo, Lintao Ma, James Y Zhang, and Jun Zhou. Timemixer: Decomposable multiscale mixing for time series forecasting. *arXiv preprint arXiv:2405.14616*, 2024b.
- Shiyu Wang, Jiawei Li, Xiaoming Shi, Zhou Ye, Baichuan Mo, Wenze Lin, Shengtong Ju, Zhixuan Chu, and Ming Jin. Timemixer++: A general time series pattern machine for universal predictive analysis. In *ICLR*, 2025.
- David H Wolpert. Stacked generalization. *Neural networks*, 5(2):241–259, 1992.
- Zhijian Xu, Ailing Zeng, and Qiang Xu. Fits: Modeling time series with  $10k$  parameters. *arXiv preprint arXiv:2307.03756*, 2024.
- Wang Xue, Tian Zhou, Qingsong Wen, Jinyang Gao, Bolin Ding, and Rong Jin. Card: Channel aligned robust blend transformer for time series forecasting. *arXiv preprint arXiv:2305.12095*, 2024.
- Kun Yi, Jingru Fei, Qi Zhang, Hui He, Shufeng Hao, Defu Lian, and Wei Fan. Filternet: Harnessing frequency filters for time series forecasting. *Advances in Neural Information Processing Systems*, 37:55115–55140, 2024.
- Guoqi Yu, Jing Zou, Xiaowei Hu, Angelica I Aviles-Rivero, Jing Qin, and Shujun Wang. Revitalizing multivariate time series forecasting: learnable decomposition with inter-series dependencies and intra-series variations modeling. In *Proceedings of the 41st International Conference on Machine Learning*, pp. 57818–57841, 2024.
- Wenzhen Yue, Yong Liu, Haoxuan Li, Hao Wang, Xianghua Ying, Ruohao Guo, Bowei Xing, and Ji Shi. Olinear: A linear model for time series forecasting in orthogonally transformed domain. *arXiv preprint arXiv:2505.08550*, 2025.
- Ailing Zeng, Muxi Chen, Lei Zhang, and Qiang Xu. Are transformers effective for time series forecasting? In *Proceedings of the AAAI conference on artificial intelligence*, volume 37, pp. 11121–11128, 2023.
- G Peter Zhang. Time series forecasting using a hybrid arima and neural network model. *Neurocomputing*, 50:159–175, 2003.
- Yunhao Zhang and Junchi Yan. Crossformer: Transformer utilizing cross-dimension dependency for multivariate time series forecasting. In *The eleventh international conference on learning representations*, 2023.
- Haoyi Zhou, Shanghang Zhang, Jieqi Peng, Shuai Zhang, Jianxin Li, Hui Xiong, and Wancai Zhang. Informer: Beyond efficient transformer for long sequence time-series forecasting. In *Proceedings of the AAAI conference on artificial intelligence*, volume 35, pp. 11106–11115, 2021.

# Appendix

## LIST OF APPENDICES

<b>A</b>	<b>Details of Datasets</b>	<b>14</b>
<b>B</b>	<b>Theoretical Analysis</b>	<b>15</b>
	B.1 Proof of the Hypothesis . . . . .	15
	B.2 Variance Analysis of Total Summed Error . . . . .	16
<b>C</b>	<b>Implicit structural Loss</b>	<b>17</b>
<b>D</b>	<b>Full Empirical Results</b>	<b>18</b>
	D.1 Long-term Forecasting Results . . . . .	18
	D.2 Short-term Forecasting Results . . . . .	18
<b>E</b>	<b>Further Ablations</b>	<b>19</b>
	E.1 The Two Principles of BDO . . . . .	19
	E.2 Preference of Deep Representations. . . . .	20
	E.3 EMA Smoothing . . . . .	21
	E.4 Pre-Dropout. . . . .	21
<b>F</b>	<b>Roubusteness</b>	<b>22</b>
<b>G</b>	<b>Visualization of Prediction</b>	<b>26</b>
<b>H</b>	<b>Limitation and Further Discussion</b>	<b>27</b>

## A DETAILS OF DATASETS

The ETTh1, ETTh2, ETTm1, and ETTm2 datasets record the temperature of electricity transformers every hour and every 15 minutes. The Weather dataset contains 21 pieces of weather information, measured every 10 minutes in Germany. The Electricity dataset records the amount of electricity used by 321 customers every hour. The Solar dataset records how much electricity is produced by solar power stations every 10 minutes, from 137 solar power stations, in 2006. The Traffic dataset records how busy the roads are in San Francisco, every hour, from 862 sensors on the freeway.

In addition, we also evaluate the short-term time series forecasting on eight multivariate datasets that are used in the study (Yue et al., 2025). The METR-LA database was populated with traffic network data for Los Angeles during the spring of 2012, specifically from March to June. This data was collected at an interval of five minutes. The NASDAQ includes the daily NASDAQ index and key economic indicators from 2010 to 2024. The SP500 records daily SP500 index data (e.g., opening price, closing price, and trading volume) from January 1993 to February 2025. CarSales collects daily sales of 10 vehicle brands (e.g., Toyota, Honda) in the U.S. from January 2005 to June 2023. The data are compiled from the Vehicle Sales dataset on Kaggle. Power contains daily wind and solar energy production (in MW) records for the French grid from April 2020 to June 2023. The data are compiled from the Wind and Solar Daily Power Production dataset on Kaggle. The website contains

Dataset	Variate	Prediction Length	Split	Frequency	domain
ETTh1, ETTh2	7	96, 192, 336, 720	(6, 2, 2)	Hourly	Electricity
ETTm1, ETTm2	7	96, 192, 336, 720	(6, 2, 2)	15min	Electricity
Weather	21	96, 192, 336, 720	(7, 1, 2)	10min	Environment
Electricity	321	96, 192, 336, 720	(7, 1, 2)	Hourly	Electricity
Traffic	862	96, 192, 336, 720	(7, 1, 2)	Hourly	Transportation
Solar	137	96, 192, 336, 720	(6, 2, 2)	10min	Energy
NASDAQ	12	24, 36, 48, 60	(7, 1, 2)	Daily	Finance
SP500	12	24, 36, 48, 60	(7, 1, 2)	Daily	Finance
Carsales	12	24, 36, 48, 60	(7, 1, 2)	Daily	Market
Website	12	24, 36, 48, 60	(7, 1, 2)	Daily	Web
Power	12	24, 36, 48, 60	(7, 1, 2)	Daily	Energy
METR-LA	207	24, 36, 48, 60	(7, 1, 2)	5min	Transportation

Table 5: Descriptions of multivariate time series datasets used in the table 6 and table 7. The Variate column represents the number of variates, and the split column specifies the train-validate-test splitting ratio for each dataset.

six years of daily visit data (e.g, first-time and returning visits) to an academic website, spanning from September 2014 to August 2020.

## B THEORETICAL ANALYSIS

### B.1 PROOF OF THE HYPOTHESIS

*Proof.* First, we derive the expected bound for each element  $y_t^{(i)}$  in a candidate forecast  $\hat{Y}_f^{(i)} = \{y_1^{(i)}, y_2^{(i)}, \dots, y_c^{(i)}\}$ , by assuming that each candidate forecast at a fixed time  $t$ , i.e.,  $\{y_t^{(i)}\}_{i=1}^c$ , are independent samples from the same distribution with  $\mathbb{E}(y_t) = \hat{\mu}_t$ .

In particular, we have

$$\mathbb{E}|\hat{\mu}_t - \frac{1}{c} \sum_{i=1}^c y_t^{(i)}|^2 = \mathbb{E}|\frac{1}{c} \sum_{i=1}^c (y_t^{(i)} - \hat{\mu}_t) + \hat{\mu}_t - \hat{\mu}_t|^2 \quad (8)$$

$$= \frac{1}{c^2} \mathbb{E}|\sum_{i=1}^c (y_t^{(i)} - \hat{\mu}_t)|^2 \quad (9)$$

$$= \frac{1}{c^2} \sum_{i=1}^c \mathbb{E}|y_t^{(i)} - \hat{\mu}_t|^2. \quad (10)$$

The last identity holds because  $\{y_t^{(i)}\}_{i=1}^c$  are independent, i.e.,  $\mathbb{E}[(y_t^{(i)} - \hat{\mu}_t)(y_t^{(j)} - \hat{\mu}_t)] = \mathbb{E}(y_t^{(i)} - \hat{\mu}_t) \cdot \mathbb{E}(y_t^{(j)} - \hat{\mu}_t) = 0, i \neq j$ .

Then, we can bound this term by showing

$$\mathbb{E}|y_t^{(i)} - \hat{\mu}_t|^2 = \mathbb{E}|y_t^{(i)} - \mathbb{E}[y_t^{(i)}]|^2 \quad (11)$$

$$= \mathbb{E}|(y_t^{(i)})^2| - |\mathbb{E}[y_t^{(i)}]|^2 \text{ (variance identity)} \quad (12)$$

$$\leq \mathbb{E}[(y_t^{(i)})^2] \leq \lambda^2. \quad (13)$$

where  $\lambda$  represents the upper bound of the second moment  $\mathbb{E}[(y_t^{(i)})^2]$ .

Therefore, we have shown that

$$\mathbb{E}|\hat{\mu}_t - \frac{1}{c} \sum_{i=1}^c y_t^{(i)}|^2 \leq \frac{\lambda^2}{c}. \quad (14)$$

for any  $i$ ; and in particular, there must exist a set of  $\{\tilde{y}_t^{(i)}\}_{i=1}^c$  satisfying

$$|\hat{\mu}_t - \frac{1}{c} \sum_{i=1}^c \tilde{y}_t^{(i)}| \leq \frac{\lambda}{\sqrt{c}}. \quad (15)$$

Fixing the set  $\{\tilde{y}_t^{(i)}\}_{i=1}^c$ , it remains to estimate the distance between the forecast by the NFM  $\Phi$  and the expected forecast  $Y_f$ , and the true observation  $X_f$ , respectively.

Since it is trivial to get

$$|\mu_t - \frac{1}{c} \sum_{i=1}^c \tilde{y}_t^{(i)}| \leq |\hat{\mu}_t - \frac{1}{c} \sum_{i=1}^c \tilde{y}_t^{(i)}| + |\hat{\mu}_t - \mu_t| \leq |\hat{\mu}_t - \frac{1}{c} \sum_{i=1}^c \tilde{y}_t^{(i)}| + b. \quad (\text{A3}) \quad (16)$$

We have

$$|x_t - \frac{1}{c} \sum_{i=1}^c \tilde{y}_t^{(i)}| \leq |\mu_t - \frac{1}{c} \sum_{i=1}^c \tilde{y}_t^{(i)}| + |x_t - \mu_t| \leq |\hat{\mu}_t - \frac{1}{c} \sum_{i=1}^c \tilde{y}_t^{(i)}| + b + \sigma. \quad (17)$$

Thus, we can derive the expected upper bound as

$$\sum_{t=1}^N |x_t - \frac{1}{c} \sum_{i=1}^c \tilde{y}_t^{(i)}| \leq N \cdot (\frac{\lambda}{\sqrt{c}} + b + \sigma) = \frac{N(\lambda + \sqrt{c}(b + \sigma))}{\sqrt{c}}. \quad (18)$$

This completes the proof.

## B.2 VARIANCE ANALYSIS OF TOTAL SUMMED ERROR

The above proof gives an intuitive bound, which does not depend on any assumption on the temporal dependence. In this part, we consider this factor as a pivot for analysing the effects of different forecasting paradigms, identifying the role of our BDO.

The variance of this total error is:

$$\text{var}(\sum_{t=1}^T e_t) = \sum_{t=1}^T \text{var}(e_t) + 2 \sum_{t < t'} \text{Cov}(e_t, e_{t'}) \quad (19)$$

For simplicity, let the prediction error at each timestep be  $e_t := \mu_t - \frac{1}{c} \sum_{i=1}^c \tilde{y}_t^{(i)}$ , and temporarily omit the effect of the predictive bias  $b$  of NFM, i.e.,  $\mu = \hat{\mu}$ . Then we can compute the covariance (autocorrelation) of the errors at any two distinct timesteps  $k$  and  $h$ ,

$$\text{Cov}(e_k, e_h) = \mathbb{E}[(\mu_k - \tilde{\mu}_k)(\mu_h - \tilde{\mu}_h)] \quad (20)$$

$$= \mathbb{E}[\tilde{\mu}_k \tilde{\mu}_h] - \mu_k \mu_h \quad (21)$$

$$= \text{Cov}(\tilde{\mu}_k, \tilde{\mu}_h) \quad (22)$$

where we denote  $\tilde{\mu}_t := \frac{1}{c} \sum_{i=1}^c \tilde{y}_t^{(i)}$ . So we have

$$\text{Cov}(\tilde{\mu}_k, \tilde{\mu}_h) = \frac{1}{c^2} \sum_{i=1}^c \sum_{j=1}^c \text{Cov}(y_k^{(i)}, y_h^{(j)}) \quad (23)$$

$$= \frac{1}{c} \text{Cov}(y_k^{(i)}, y_h^{(i)}), \forall i \quad (24)$$

The last inequality holds by isolating the correlations across different candidates.

Now we can consider the role of temporal dependence in the error structure.

**Case 1: Temporal Independence (The DO Paradigm):** The DO paradigm is designed to (approximately) satisfy the assumption of temporal independence, as evidenced in Sec. 2. This implies that the error covariance terms in Eq. 24 are (nearly) zero. Consequently, the total error variance is simply the sum of the per-timestep variances, While this structure effectively prevents the compounding of

errors, it often comes at the cost of the model being "unaware" of the sequential dynamics within the future horizon, potentially leading to higher per-timestep variance.

**Case 2: Temporal Dependence (The AR Paradigm).** : The typical AR paradigm fundamentally violates this assumption and thus leads to errors from one step propagating to the next, which causes the total variance to explode over long horizons. Even though the introduction of the ensembling factor  $c$  would reduce the magnitude of this effect, it does not alter the underlying structural problem of error accumulation.

**Case 3: A Synthesis (The BDO Paradigm).**: Our Boosted Direct Output paradigm operates as a synthesis of these two extremes. It intentionally violates strict temporal independence by recursively feeding sub-forecasts back into the model, thereby making it aware of causal dependencies within the forecast horizon. However, unlike a pure AR model, through hierarchical supervision and its patch-wise output structure inherited from DO, the model is trained to control the accumulation of errors. The goal is to leverage the benefits of modeling temporal structure while constraining the error correlation, effectively learning to make the covariance term in Eq. 24 as small as possible.

Note that the above proof and analysis are based on a univariate time series; however, it is easy to extend the result to the multivariate case using a similar process in a certain normed vector space.

## C IMPLICIT STRUCTURAL LOSS

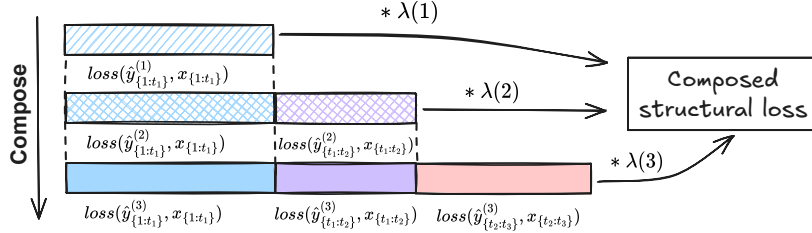


Figure 10: Illustration of the implicit structural loss of BDO, we exemplify it in the NF consisting of three sub-forecasters.

An interesting property of the BDO paradigm is the implicit structural loss it induces. This connects our work to recent research on explicit loss engineering, such as positional weighting (Xue et al., 2024) and patch-wise structural losses (Kudrat et al., 2025). We posit that the BDO learning objective, formed by the weighted sum of losses from hierarchical sub-forecasts, inherently functions as a complex structural loss. This seemingly implicit loss can be seen as the generalized version of the above two.

To formalize this property, we first simplify the loss function from Eq.6 as:

$$Loss = \sum_{n=1}^N \lambda(n) * f(\hat{Y}_f^{(n)}, X_f^{(n)}) \quad (25)$$

where  $f(\cdot, \cdot)$  denotes a base error function such as the MAE.

Note that in our definitions and notations,  $\hat{Y}_f^{(n)} = \{\hat{y}_1^{(n)}, \hat{y}_2^{(n)}, \dots, \hat{y}_{t_n}^{(n)}\}$ . We can therefore expand the total loss into a point-wise sum over all timesteps:

$$Loss = \sum_{n=1}^N \sum_{t=1}^{t_n} \lambda(n) * f(\hat{y}_t^{(n)}, x_t) \quad (26)$$

The underlying structure of this composite loss, visualized in Figure 10, reveals a key insight: BDO is not just a recursive forecasting process, but also a method for implicitly constructing a complex and adaptive structural loss. The properties of this loss can be finely tuned through several mechanisms: the stage-wise weighting coefficients, the forecast splitting strategy, the choice of the base error function, and even the architecture of each sub-forecaster.

## D FULL EMPIRICAL RESULTS

### D.1 LONG-TERM FORECASTING RESULTS

We present the full version of Table.2 in Table.6 to show the capability of ReNF in Long-Term time series forecasting.

Models	Re-Bound		ReNF		TimeBridge		DUET		TimeDistill		Timer-XL		iTransformer		TimeMixer		PatchTST		Crossformer		DLinear		
	MSE	MAE	MSE	MAE	MSE	MAE	MSE	MAE	MSE	MAE	MSE	MAE	MSE	MAE	MSE	MAE	MSE	MAE	MSE	MAE	MSE	MAE	
Weather	96	0.110	0.149	<b>0.138</b>	<b>0.180</b>	<u>0.144</u>	<u>0.184</u>	0.146	0.191	0.145	0.204	0.157	0.205	0.157	0.206	0.147	0.198	0.150	0.200	0.143	0.210	0.170	0.230
	192	0.141	0.185	<b>0.182</b>	<b>0.224</b>	<u>0.186</u>	<u>0.226</u>	0.188	0.231	0.188	0.247	0.206	0.250	0.200	0.248	0.192	0.242	0.191	0.239	0.195	0.261	0.216	0.273
	336	0.177	0.216	<b>0.231</b>	<b>0.266</b>	<u>0.237</u>	<u>0.267</u>	<u>0.235</u>	0.269	0.240	0.286	0.259	0.291	0.252	0.287	0.247	0.284	0.242	0.279	0.254	0.319	0.258	0.307
	720	0.232	0.261	<b>0.304</b>	<b>0.318</b>	0.312	<u>0.321</u>	<u>0.308</u>	<u>0.319</u>	0.310	0.338	0.337	0.344	0.320	0.336	0.318	0.330	0.312	0.330	0.335	0.385	0.323	0.362
	Avg.	0.165	0.203	<b>0.214</b>	<b>0.247</b>	0.220	<u>0.250</u>	<u>0.219</u>	0.253	0.221	0.269	0.240	0.273	0.232	0.269	0.226	0.264	0.224	0.262	0.232	0.294	0.242	0.293
Electricity	96	0.083	0.171	<b>0.118</b>	<b>0.210</b>	<u>0.122</u>	<u>0.216</u>	0.128	0.219	0.128	0.225	0.127	0.219	0.134	0.230	0.153	0.256	0.143	0.247	0.134	0.231	0.140	0.237
	192	0.097	0.186	<b>0.138</b>	<b>0.229</b>	<u>0.143</u>	0.238	0.145	<u>0.235</u>	0.145	0.241	0.145	0.236	0.154	0.250	0.168	0.269	0.158	0.261	0.146	0.243	0.154	0.251
	336	0.105	0.196	<b>0.151</b>	<b>0.244</b>	<u>0.163</u>	0.258	0.163	<u>0.255</u>	0.161	0.258	0.159	0.252	0.169	0.265	0.189	0.291	0.168	0.267	0.165	0.264	0.169	0.268
	720	0.115	0.207	<b>0.173</b>	<b>0.266</b>	<u>0.178</u>	<u>0.274</u>	0.193	0.281	0.195	0.291	0.187	0.277	0.194	0.288	0.228	0.320	0.214	0.307	0.237	0.314	0.204	0.301
	Avg.	0.100	0.190	<b>0.145</b>	<b>0.237</b>	<u>0.152</u>	<u>0.247</u>	0.157	0.248	0.157	0.254	0.155	0.246	0.163	0.258	0.185	0.284	0.171	0.271	0.171	0.263	0.167	0.264
Traffic	96	0.234	0.167	<u>0.335</u>	<b>0.226</b>	<u>0.332</u>	<u>0.237</u>	0.360	0.238	0.358	0.256	0.340	0.238	0.358	0.258	0.369	0.257	0.370	0.262	0.526	0.288	0.395	0.275
	192	0.245	0.175	<u>0.356</u>	<u>0.239</u>	<b>0.343</b>	<b>0.239</b>	0.383	0.249	0.374	0.264	0.360	0.248	0.382	0.271	0.399	0.272	0.386	0.269	0.503	0.263	0.407	0.280
	336	0.254	0.180	<u>0.366</u>	<b>0.246</b>	<b>0.360</b>	<u>0.249</u>	0.395	0.259	0.389	0.271	0.377	0.256	0.396	0.277	0.407	0.272	0.396	0.275	0.505	0.276	0.417	0.286
	720	0.284	0.197	<u>0.402</u>	<b>0.267</b>	<b>0.392</b>	<u>0.268</u>	0.435	0.278	0.428	0.292	0.418	0.279	0.445	0.308	0.461	0.316	0.435	0.295	0.552	0.301	0.454	0.308
	Avg.	0.254	0.180	<u>0.365</u>	<b>0.245</b>	<b>0.357</b>	<u>0.248</u>	0.393	0.256	0.387	0.271	0.374	0.255	0.395	0.279	0.409	0.279	0.397	0.275	0.522	0.282	0.418	0.287
Solar	96	0.082	0.141	<b>0.157</b>	<u>0.202</u>	<u>0.159</u>	<b>0.196</b>	0.166	0.211	0.166	0.229	0.162	0.221	0.190	0.244	0.179	0.232	0.170	0.234	0.183	0.208	0.199	0.265
	192	0.087	0.145	<u>0.174</u>	<b>0.210</b>	<b>0.173</b>	<u>0.215</u>	0.199	0.212	0.181	0.239	0.187	0.239	0.193	0.257	0.201	0.259	0.204	0.302	0.208	0.227	0.220	0.281
	336	0.099	0.156	<b>0.180</b>	<u>0.219</u>	0.193	0.229	0.207	<b>0.215</b>	<u>0.191</u>	0.246	0.205	0.255	0.203	0.266	0.190	0.256	0.212	0.293	0.212	0.239	0.234	0.295
	720	0.092	0.151	<b>0.190</b>	<u>0.225</u>	<u>0.207</u>	<u>0.237</u>	0.206	<b>0.217</b>	0.199	0.252	0.238	0.279	0.223	0.281	0.203	0.261	0.215	0.307	0.215	0.256	0.243	0.301
	Avg.	0.090	0.148	<b>0.176</b>	<b>0.214</b>	<u>0.183</u>	0.219	0.195	<u>0.214</u>	0.184	0.242	0.198	0.249	0.202	0.262	0.193	0.252	0.200	0.284	0.205	0.233	0.224	0.286
ETTm1	96	0.189	0.262	<b>0.270</b>	<b>0.325</b>	0.288	0.339	<u>0.279</u>	<u>0.333</u>	0.285	0.344	0.290	0.341	0.300	0.353	0.293	0.345	0.289	0.342	0.314	0.367	0.300	0.345
	192	0.218	0.284	<b>0.310</b>	<b>0.352</b>	0.326	0.368	<u>0.320</u>	<u>0.358</u>	0.331	0.368	0.337	0.369	0.341	0.380	0.335	0.372	0.329	0.368	0.374	0.410	0.336	0.366
	336	0.242	0.300	<b>0.343</b>	<b>0.373</b>	0.363	0.394	<u>0.348</u>	<u>0.377</u>	0.359	0.386	0.374	0.393	0.374	0.396	0.368	0.386	0.362	0.390	0.413	0.432	0.367	0.387
	720	0.249	0.296	<b>0.400</b>	<b>0.405</b>	0.417	0.419	<u>0.405</u>	<u>0.408</u>	0.415	0.416	0.437	0.428	0.429	0.430	0.426	0.417	0.416	0.423	0.753	0.613	0.419	0.417
	Avg.	0.225	0.286	<b>0.331</b>	<b>0.364</b>	0.349	0.380	<u>0.338</u>	<u>0.369</u>	0.348	0.380	0.359	0.382	0.361	0.390	0.356	0.380	0.349	0.381	0.464	0.456	0.356	0.379
ETTm2	96	0.131	0.214	<b>0.157</b>	<b>0.241</b>	<u>0.157</u>	<u>0.243</u>	0.162	0.249	0.163	0.255	0.175	0.257	0.175	0.266	0.165	0.256	0.165	0.255	0.296	0.391	0.164	0.256
	192	0.174	0.246	<b>0.212</b>	<b>0.279</b>	0.218	<u>0.284</u>	<u>0.215</u>	0.288	0.220	0.294	0.242	0.301	0.242	0.312	0.225	0.298	0.221	0.293	0.369	0.416	0.224	0.304
	336	0.216	0.276	<b>0.262</b>	<b>0.315</b>	0.270	<u>0.321</u>	<u>0.267</u>	0.321	0.269	0.328	0.293	0.337	0.282	0.337	0.277	0.332	0.276	0.327	0.588	0.600	0.277	0.337
	720	0.283	0.322	<b>0.341</b>	<b>0.368</b>	<u>0.344</u>	0.372	0.348	0.373	0.346	<u>0.369</u>	0.376	0.390	0.375	0.394	0.360	0.385	0.362	0.381	0.750	0.612	0.371	0.401
	Avg.	0.201	0.265	<b>0.243</b>	<b>0.301</b>	<u>0.247</u>	<u>0.305</u>	0.248	0.308	0.250	0.312	0.271	0.322	0.269	0.327	0.257	0.318	0.256	0.314	0.501	0.505	0.259	0.325
ETTth1	96	0.243	0.300	<b>0.350</b>	<b>0.383</b>	0.355	0.391	<u>0.353</u>	<u>0.386</u>	0.373	0.401	0.364	0.397	0.386	0.405	0.372	0.401	0.377	0.397	0.411	0.435	0.379	0.403
	192	0.276	0.327	<b>0.385</b>	<b>0.408</b>	<u>0.389</u>	0.414	0.398	<u>0.409</u>	0.411	0.426	0.405	0.424	0.424	0.440	0.413	0.429	0.409	0.425	0.409	0.438	0.408	0.419
	336	0.294	0.342	<b>0.405</b>	<b>0.425</b>	<u>0.415</u>	0.435	0.415	<u>0.428</u>	0.439	0.446	0.427	0.439	0.449	0.460	0.438	0.450	0.431	0.444	0.433	0.457	0.440	0.440
	720	0.266	0.322	<b>0.422</b>	<b>0.449</b>	<u>0.443</u>	0.462	0.436	<u>0.458</u>	0.495	0.493	0.439	0.459	0.495	0.487	0.486	0.484	0.457	0.477	0.501	0.514	0.471	0.493
	Avg.	0.270	0.323	<b>0.391</b>	<b>0.416</b>	<u>0.401</u>	0.426	0.401	<u>0.420</u>	0.430	0.441	0.409	0.430	0.439	0.448	0.427	0.441	0.419	0.436	0.439	0.461	0.425	0.439
ETTm2	96	0.214	0.285	<b>0.261</b>	<b>0.329</b>	<u>0.270</u>	<u>0.331</u>	0.271	0.335	0.273	0.336	0.277	0.343	0.297	0.348	0.281	0.351	0.274	0.337	0.728	0.603	0.300	0.364
	192	0.261	0.320	<b>0.320</b>	<b>0.370</b>	0.338	<u>0.375</u>	<u>0.335</u>	0.376	0.334	0.381	0.348	0.391	0.372	0.403	0.349	0.387	0.348	0.384	0.723	0.607	0.387	0.423
	336	0.270	0.327	<b>0.346</b>	<b>0.394</b>	0.370	0.402	<u>0.354</u>	<u>0.398</u>	0.363	0.415	0.375	0.418	0.388	0.418	0.366	0.413	0.377	0.416	0.740	0.628	0.490	0.487
	720	0.261	0.325	<b>0.381</b>	<b>0.423</b>	0.402	0.434	<u>0.384</u>	<u>0.426</u>	0.408	0.446	0.409	0.458	0.424	0.444	0.401	0.436	0.406	0.441	1.386	0.882	0.704	0.597
	Avg.	0.252	0.314	<b>0.327</b>	<b>0.379</b>	0.345	0.386	<u>0.336</u>	<u>0.384</u>	0.345	0.395	0.352	0.402	0.370	0.403	0.349	0.397	0.351	0.395	0.894	0.680	0.470	0.468

Table 6: Full results of long-term forecasting of hyperparameter searching. The Re-Bound column denotes the empirical bound discussed in Sec.3.3. The look-back window is searched from {336, 512, 720} for the best performance. Timer-XL uses a 672-length window as in the original paper. All results are averaged across four different prediction lengths: {96, 192, 336, 720}. The **best** and **second-best** results are highlighted.

### D.2 SHORT-TERM FORECASTING RESULTS

To further demonstrate the generality of ReNF, we test it at six supplementary datasets from a recent short-term time series forecasting benchmark (Yue et al., 2025). The descriptions of these datasets can be found in the Table.5. As shown in Table 7, ReNF remains highly competitive against recent state-of-the-art models in short-term forecasting tasks. However, the performance advantage is less pronounced than in the LTSF setting, a result that aligns with the design principles of BDO. First, when restricted to the shorter look-back windows typical of short-term tasks, the initial forecasts in

Model	ReNF	OLinear	TimeMix.	FilterNet	FITS	DLinear	TimeMix.++	Leddam	CARD	Fredformer	iTrans.	PatchTST													
	(Ours)	2025	2024b	2024	2024	2023	2025	2024	2024	2024	2024	2023													
Metric	MSE	MAE	MSE	MAE	MSE	MAE	MSE	MAE	MSE	MAE	MSE	MAE													
CuSites	24	<b>0.263</b>	<b>0.283</b>	0.320	<u>0.302</u>	0.320	0.318	0.318	0.319	0.359	0.347	0.354	0.350	0.323	0.320	0.325	0.322	0.337	0.321	0.319	0.326	<u>0.303</u>	0.312	0.319	0.319
	36	<b>0.280</b>	<b>0.298</b>	0.334	<u>0.315</u>	0.332	0.331	0.331	0.330	0.373	0.360	0.368	0.365	0.351	0.348	0.337	0.333	0.348	0.333	0.333	0.335	<u>0.318</u>	0.323	0.332	0.330
	48	<b>0.299</b>	<b>0.315</b>	0.347	<u>0.327</u>	0.345	0.343	0.342	0.341	0.385	0.370	0.382	0.379	0.351	0.342	0.351	0.346	0.362	0.345	0.349	0.344	<u>0.331</u>	0.332	0.347	0.344
	60	<b>0.315</b>	<b>0.328</b>	0.358	<u>0.337</u>	0.355	0.351	0.352	0.349	0.399	0.385	0.388	0.380	0.363	0.352	0.361	0.353	0.372	0.353	0.359	0.349	<u>0.344</u>	0.342	0.355	0.348
	Avg	<b>0.289</b>	<b>0.306</b>	0.340	<u>0.320</u>	0.338	0.336	0.336	0.335	0.379	0.365	0.373	0.368	0.347	0.340	0.343	0.338	0.355	0.338	0.340	0.338	<u>0.324</u>	0.327	0.338	0.335
Power	24	<b>1.268</b>	<b>0.855</b>	1.343	<u>0.870</u>	1.341	0.881	1.410	0.916	1.491	0.944	1.390	0.916	<u>1.340</u>	0.877	1.397	0.909	1.406	0.886	1.410	0.913	1.462	0.924	1.468	0.935
	36	<b>1.336</b>	<b>0.880</b>	1.445	<u>0.903</u>	<u>1.420</u>	0.914	1.590	0.968	1.621	0.994	1.518	0.957	1.446	0.920	1.509	0.951	1.506	0.921	1.538	0.953	1.582	0.964	1.593	0.972
	48	<b>1.354</b>	<b>0.893</b>	1.559	0.946	1.567	0.963	1.680	1.009	1.775	1.052	1.610	0.995	<u>1.467</u>	<u>0.933</u>	1.646	0.999	1.583	0.957	1.652	1.008	1.696	1.011	1.710	1.020
	60	<b>1.383</b>	<b>0.913</b>	<u>1.602</u>	<u>0.971</u>	1.609	0.988	1.776	1.053	1.958	1.122	1.679	1.020	1.626	1.006	1.727	1.043	1.693	1.003	1.752	1.049	1.796	1.061	1.829	1.064
	Avg	<b>1.335</b>	<b>0.885</b>	1.487	<u>0.922</u>	1.484	0.937	1.614	0.986	1.711	1.028	1.549	0.972	<u>1.470</u>	0.934	1.570	0.975	1.547	0.942	1.588	0.981	1.634	0.990	1.650	0.998
METR-LA	24	<b>0.613</b>	<u>0.348</u>	0.650	<b>0.337</b>	0.671	0.413	0.670	0.402	0.698	0.416	0.645	0.458	<u>0.617</u>	0.394	0.680	0.405	0.700	0.378	0.676	0.408	0.700	0.413	0.679	0.410
	36	<b>0.748</b>	<u>0.398</u>	0.800	<b>0.388</b>	0.841	0.480	0.824	0.471	0.874	0.490	0.785	0.533	<u>0.781</u>	0.457	0.841	0.471	0.874	0.448	0.852	0.477	0.867	0.480	0.845	0.484
	48	<u>0.860</u>	<u>0.438</u>	0.905	<b>0.427</b>	0.964	0.531	0.955	0.521	1.013	0.546	0.885	0.585	<b>0.842</b>	0.520	0.963	0.528	1.017	0.498	0.982	0.526	1.017	0.539	0.972	0.536
	60	<b>0.950</b>	<u>0.471</u>	0.999	<b>0.457</b>	1.047	0.573	1.050	0.563	1.122	0.589	0.959	0.623	<u>0.958</u>	0.551	1.029	0.556	1.126	0.541	1.084	0.569	1.079	0.572	1.077	0.578
	Avg	<b>0.793</b>	<u>0.414</u>	0.838	<b>0.402</b>	0.881	0.499	0.875	0.489	0.927	0.510	0.819	0.550	<u>0.799</u>	0.480	0.878	0.490	0.929	0.466	0.898	0.495	0.916	0.501	0.893	0.502
Website	24	<b>0.155</b>	<b>0.286</b>	0.186	0.306	0.229	0.335	0.273	0.357	0.431	0.469	0.315	0.393	0.231	0.349	0.240	0.345	0.325	0.370	0.216	0.335	<u>0.181</u>	<u>0.305</u>	0.245	0.350
	36	<b>0.224</b>	<b>0.343</b>	0.272	0.356	0.361	0.420	0.401	0.441	0.554	0.552	0.385	0.447	0.328	0.397	0.327	0.405	0.428	0.442	0.331	0.411	<u>0.226</u>	<u>0.343</u>	0.370	0.429
	48	<u>0.283</u>	<u>0.386</u>	0.365	0.391	0.501	0.507	0.530	0.522	0.694	0.647	0.436	0.486	0.450	0.473	0.446	0.475	0.457	0.478	0.483	0.496	<b>0.263</b>	<b>0.370</b>	0.504	0.513
	60	<b>0.267</b>	<b>0.374</b>	0.486	0.481	0.571	0.562	0.630	0.592	0.736	0.673	0.468	0.510	0.525	0.517	0.561	0.549	0.596	0.566	0.556	0.547	<b>0.323</b>	<b>0.410</b>	0.587	0.565
	Avg	<b>0.233</b>	<b>0.348</b>	0.327	0.383	0.415	0.456	0.458	0.478	0.604	0.585	0.401	0.459	0.384	0.434	0.393	0.443	0.451	0.464	0.396	0.447	<u>0.248</u>	<u>0.357</u>	0.426	0.464
SP500	24	<b>0.150</b>	<b>0.270</b>	0.155	<u>0.271</u>	0.159	0.288	0.181	0.317	0.193	0.334	0.189	0.330	0.172	0.305	0.175	0.308	<u>0.156</u>	0.276	0.181	0.315	0.180	0.309	0.164	0.298
	36	<b>0.204</b>	<u>0.322</u>	0.209	<b>0.317</b>	0.218	0.343	0.224	0.341	0.259	0.389	0.250	0.363	0.227	0.344	0.232	0.358	<u>0.206</u>	0.319	0.239	0.365	0.225	0.346	0.221	0.341
	48	<b>0.251</b>	<u>0.355</u>	<u>0.258</u>	0.358	0.264	0.367	0.280	0.384	0.324	0.439	0.291	0.398	0.272	0.383	0.276	0.388	<u>0.258</u>	<b>0.354</b>	0.283	0.394	0.275	0.383	0.278	0.397
	60	<b>0.295</b>	<b>0.386</b>	0.305	<u>0.387</u>	0.322	0.416	0.332	0.416	0.391	0.486	0.377	0.475	0.319	0.413	0.325	0.423	<u>0.303</u>	<b>0.385</b>	0.341	0.438	0.322	0.418	0.321	0.409
	Avg	<b>0.225</b>	<b>0.333</b>	<u>0.231</u>	<b>0.333</b>	0.241	0.353	0.254	0.365	0.291	0.412	0.277	0.391	0.247	0.361	0.252	0.369	<u>0.231</u>	<b>0.333</b>	0.261	0.378	0.250	0.364	0.246	0.361
NASDAQ	24	<b>0.114</b>	<b>0.211</b>	0.121	0.216	<u>0.122</u>	0.221	0.130	0.230	0.140	0.244	0.155	0.274	0.132	0.233	0.125	0.222	0.124	<u>0.220</u>	0.128	0.226	0.137	0.237	0.127	0.224
	36	<b>0.155</b>	<b>0.253</b>	<u>0.163</u>	<u>0.261</u>	0.183	0.279	0.175	0.273	0.184	0.284	0.196	0.306	0.177	0.278	0.174	0.271	0.167	0.266	0.170	0.268	0.184	0.280	0.174	0.269
	48	<b>0.196</b>	<b>0.290</b>	0.205	0.296	<u>0.200</u>	<u>0.298</u>	0.224	0.314	0.234	0.324	0.244	0.344	0.216	0.311	0.222	0.312	0.218	0.307	0.218	0.306	0.229	0.318	0.225	0.314
	60	<b>0.236</b>	<b>0.321</b>	0.259	0.336	<u>0.238</u>	<u>0.328</u>	0.259	0.340	0.282	0.357	0.318	0.401	0.249	0.337	0.264	0.341	0.264	0.341	0.262	0.339	0.279	0.352	0.265	0.339
	Avg	<b>0.175</b>	<b>0.269</b>	0.187	0.277	<u>0.186</u>	<u>0.281</u>	0.197	0.289	0.210	0.302	0.228	0.331	0.193	0.290	0.196	0.286	0.193	0.284	0.194	0.285	0.207	0.297	0.198	0.286

Table 7: Full results for the short-term forecasting. We use the look-back window with length  $T = 36$  to predict lengths  $\{24, 36, 48, 60\}$ . The **best results** and **second-best results** are highlighted.

the BDO process are inherently less accurate. Consequently, recursively combining these noisier predictions can offset the benefits of the paradigm. Second, the hierarchical curriculum learning of BDO yields diminishing returns on short horizons; the strategy of decomposing a short prediction interval into even smaller sub-forecasts becomes redundant. We provide a more rigorous verification of these dynamics in Sec. E.1, where we conduct ablation studies on the BDO module using the M4 and PEMS datasets.

From another perspective, while our proposed methods are universally applicable, these results also highlight the value of more specialized or refined extensions of our proposals in further enhancing the capabilities of BDO in various scenarios.

## E FURTHER ABLATIONS

### E.1 THE TWO PRINCIPLES OF BDO

We posit that our BDO paradigm derives its efficacy from two distinct and essential mechanisms: (1) block-wise Supervision, which generates explicit sub-forecasts from intermediate representations at each stage; and (2) Recursive Concatenation, which feeds these sub-forecasts back into the input of the subsequent stage, encouraging the network to implicitly learn a post-combination function. To disentangle their respective contributions across diverse forecasting tasks, we conduct ablation studies on these two factors.

**Multivariate Long-Term Forecasting:** Table 8 presents the ablation results on the Electricity, ETTh1, and ETTm1 datasets. The results indicate that the two components are synergistic; removing either leads to a notable degradation in performance. Overall, we observe that hierarchical supervision plays the dominant role in this setting. This is expected, as it not only facilitates the repeated reuse of label information but also enforces a causal and homogeneous structure on the predictive representations across layers—an effect visualized in Figure 12.

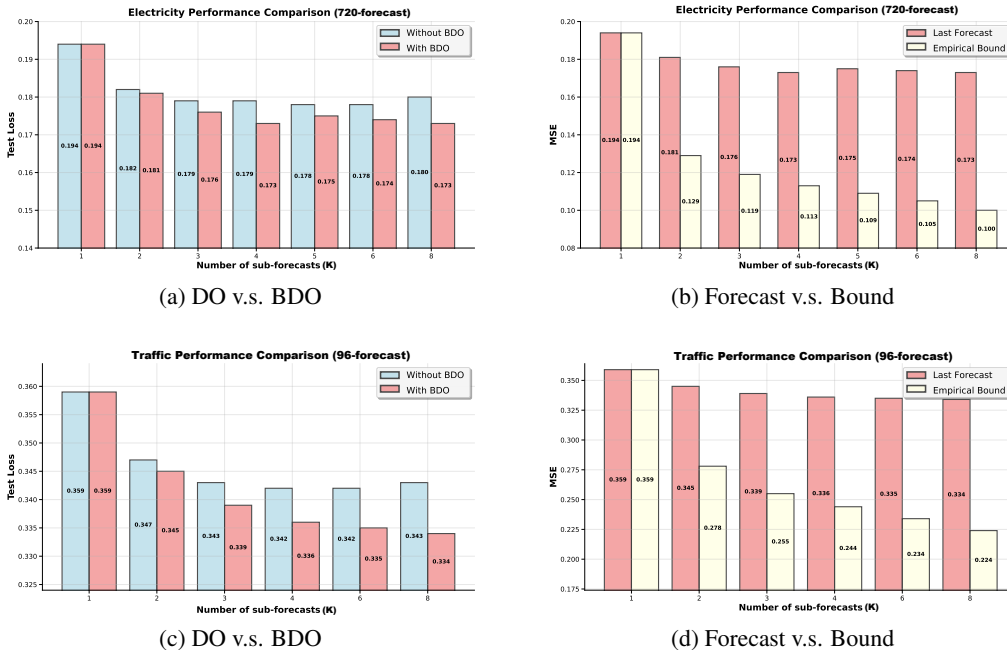


Figure 11: Supplementary illustrations of the performance variation with different numbers of sub-forecasts  $K$ . (a). Comparison of using DO or BDO with the Electricity dataset. (b). Comparison between the best forecast and the empirical bound of ReNF with the Electricity dataset. (c). Comparison of using DO or BDO with the Traffic dataset. (d). Comparison between the best forecast and the empirical bound of ReNF with the Traffic dataset.

**Short-Term Forecasting:** We extend this analysis to short-term tasks using the multivariate PEMS datasets (PEMS03, PEMS08) and the univariate M4 dataset (Yearly, Quarterly, Monthly). For the M4 dataset, we adapt our strategy due to its specific characteristics (fixed, short horizons, and heterogeneous series). We set the length of each sub-forecast equal to the full forecasting horizon. This disables the short-to-long curriculum aspect of block-wise supervision, but keeps the function of implicit forecast combination. As shown in Figure 13, both components remain effective. However, in stark contrast to the long-term setting, the contribution of block-wise supervision is diminished. This aligns with our discussion in Section D.2: when the horizon is short, intermediate supervision steps may introduce auto-regressive noise and error that outweigh the information gain. To verify this hypothesis, Figure 13 illustrates the variation of performance gain provided by block-wise supervision as the forecasting horizon increases. We compare two settings on the PEMS datasets: (1) a short-term setting (forecasting 12, 24, 48 steps given 96 steps) and (2) a long-term setting (forecasting 96, 192, 336 steps given 512 steps). The results clearly show that as the task switches to long-term forecasting, the benefits of block-wise supervision become significant. This confirms that the full BDO paradigm, including its curriculum supervision, is most potent when the input and output contexts are sufficiently long.

## E.2 PREFERENCE OF DEEP REPRESENTATIONS.

In Sec. 2.3, we introduce two variants of MLPs with a few differences. The primary distinction is the inclusion of skip-connections between representations in ReNF- $\beta$ , which facilitates the learning of deeper, more complex non-linear dynamics. To justify this design choice, the following experiments demonstrate the performance degradation that occurs when a model’s complexity is mismatched with the dataset’s intrinsic characteristics.

Specifically, we apply the ReNF- $\beta$  to the ETTh1 and ETTh2 datasets, and apply the alpha version to the large volume Electricity and Traffic datasets. The results are shown in the Table 9, from which we can deduce that the complex deep representations of ReNF- $\beta$  are clearly detrimental to ETTh datasets. In stark contrast, large-volume datasets like Electricity and Traffic benefit from deeper,

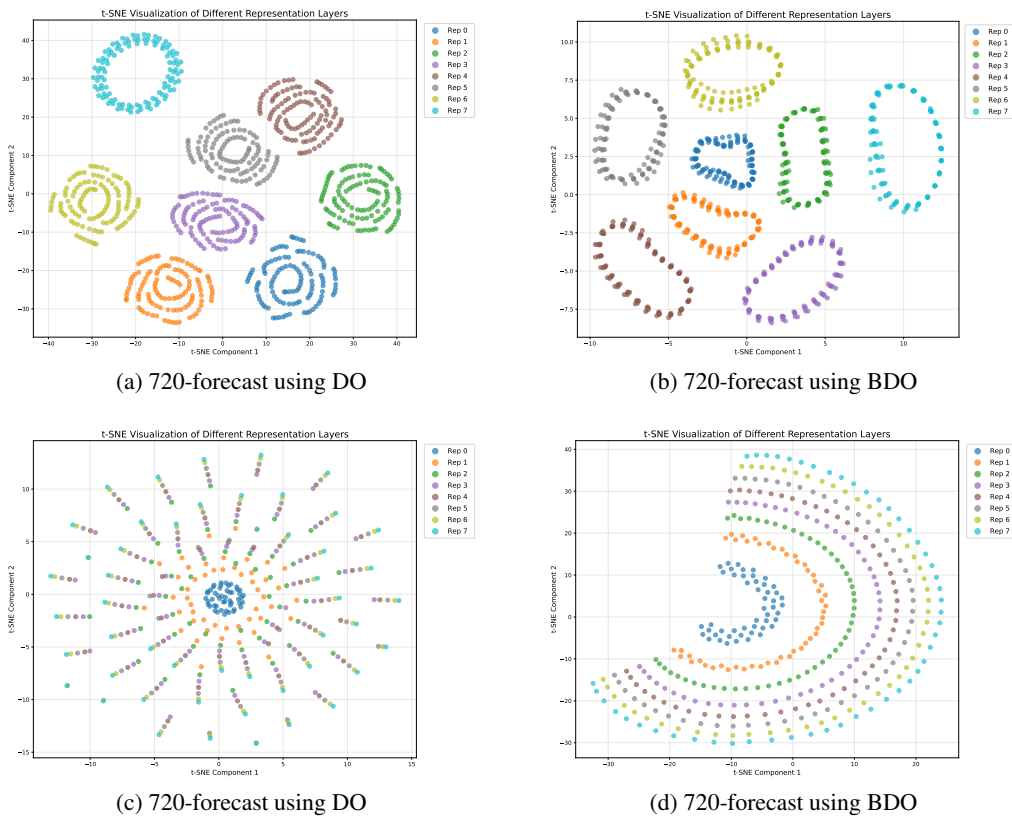


Figure 12: Visualizations of the representations of different layers/sub-forecasters. (a). representations of using DO with the ETTh1 dataset. (b). representations of using BDO with the ETTh1 dataset. (c). representations of using DO with the ETTm1 dataset. (d). representations of using BDO with the ETTm1 dataset. This indicates that BDO tends to form predictive representations that are homogeneous and hierarchical.

more expressive representations. This finding provides a direct explanation, from the perspective of representation depth, for the recurring phenomenon where simpler, parsimonious NFs outperform more complex ones on certain benchmarks. It underscores the critical importance of matching model capacity to the intrinsic characteristics of the time series data, identifying a clear direction for future work in adaptive forecaster design.

### E.3 EMA SMOOTHING

The results in Table 10 confirm that EMA smoothing yields substantial improvements in final forecast accuracy. This empirically validates our hypothesis from Section 2: EMA mitigates the detrimental effects of flawed early stopping, where volatile validation scores lead to the premature saving of suboptimal models. By providing a more reliable and stable training signal, EMA not only enhances performance but also establishes the robust foundation necessary to fairly evaluate our other contributions, such as the BDO paradigm.

### E.4 PRE-DROPOUT.

Our MLP architecture applies dropout to the input data by default as a regularization technique. While its impact can be subtle and dataset-dependent, we perform an ablation study for the sake of completeness. The results of this analysis on the ETTh1, ETTh2, and Electricity datasets are presented in Table 11.

Method	ReNF (Ours)		w/o Concat		w/o Supervision		
	MSE	MAE	MSE	MAE	MSE	MAE	
Electricity	96	<b>0.118</b>	<b>0.210</b>	0.119	0.211	0.123	0.215
	192	<b>0.138</b>	<b>0.229</b>	0.138	0.229	0.145	0.236
	336	<b>0.151</b>	<b>0.244</b>	0.153	0.245	0.156	0.251
	720	<b>0.173</b>	<b>0.266</b>	0.179	0.271	0.177	0.269
	Avg.	<b>0.145</b>	<b>0.237</b>	0.147	0.239	0.150	0.243
ETTh1	96	<b>0.350</b>	0.383	0.356	<b>0.382</b>	0.356	<b>0.382</b>
	192	<b>0.385</b>	0.408	0.394	<b>0.406</b>	0.394	0.407
	336	<b>0.405</b>	<b>0.427</b>	0.420	0.427	0.420	0.425
	720	<b>0.422</b>	<b>0.449</b>	0.432	0.454	0.436	0.456
	Avg.	<b>0.391</b>	<b>0.416</b>	0.400	0.417	0.402	0.418
ETTm1	96	<b>0.270</b>	<b>0.325</b>	0.273	0.327	0.275	0.327
	192	<b>0.310</b>	<b>0.352</b>	0.311	0.355	0.312	0.353
	336	0.343	<b>0.373</b>	0.343	0.376	<b>0.342</b>	0.374
	720	0.401	<b>0.406</b>	<b>0.398</b>	0.409	0.413	0.410
	Avg.	<b>0.331</b>	<b>0.364</b>	<b>0.331</b>	0.367	0.336	0.366
Solar	96	<b>0.157</b>	0.202	0.165	<b>0.201</b>	0.170	0.217
	192	<b>0.174</b>	<b>0.210</b>	0.185	0.215	0.195	0.226
	336	<b>0.180</b>	<b>0.219</b>	0.185	<b>0.219</b>	0.189	0.233
	720	<b>0.190</b>	<b>0.225</b>	0.197	0.227	0.197	0.238
	Avg.	<b>0.176</b>	<b>0.214</b>	0.183	0.216	0.188	0.229

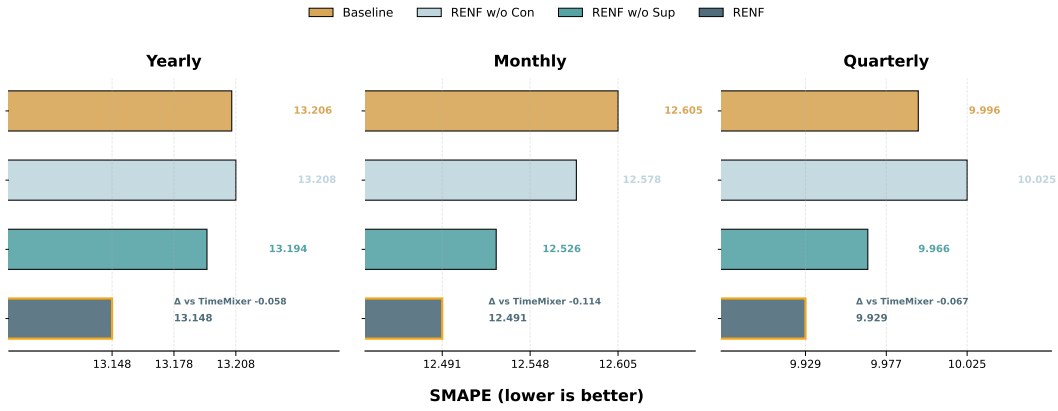
Table 8: Ablation study on the core components of BDO. 'Concat' denotes recursive concatenation in input space; 'Supervision' denotes block-wise supervision. The best results are highlighted in **bold**.

## F ROBUSTNESS

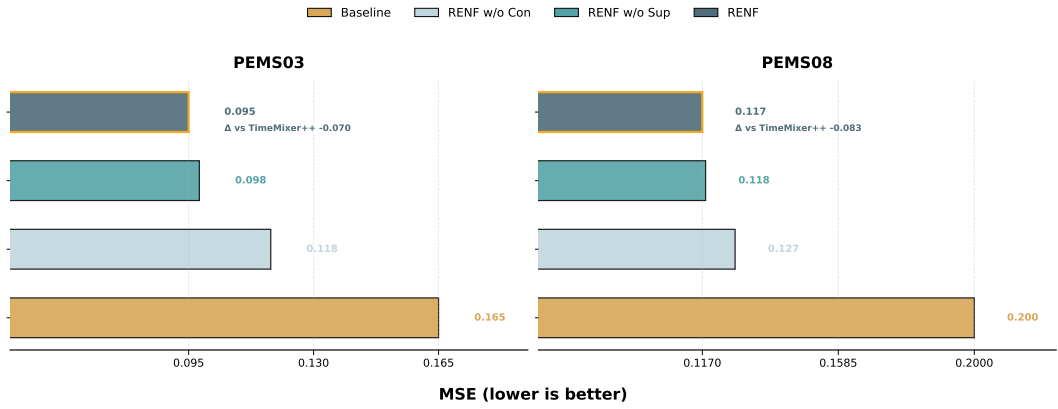
In Table 12, we present the error bar of ReNF in datasets with relatively small sizes or high instability. It shows that ReNF exhibits high robustness because of its simple structure and inherent variance reduction, which is a favorable characteristic for industrial applications.

Dataset	ReNF (Origin)		ReNF (Exchange)		
	MSE	MAE	MSE	MAE	
ETTh1	96	<b>0.350</b>	<b>0.383</b>	0.384	0.410
	192	<b>0.385</b>	<b>0.408</b>	0.407	0.428
	336	<b>0.405</b>	<b>0.425</b>	0.447	0.456
	720	<b>0.422</b>	<b>0.449</b>	0.502	0.493
	Avg.	<b>0.391</b>	<b>0.416</b>	0.435	0.447
ETTh2	96	<b>0.261</b>	<b>0.329</b>	0.271	0.332
	192	<b>0.320</b>	<b>0.370</b>	0.340	0.376
	336	<b>0.346</b>	<b>0.394</b>	0.381	0.410
	720	<b>0.381</b>	<b>0.423</b>	0.415	0.437
	Avg.	<b>0.327</b>	<b>0.379</b>	0.352	0.389
Electricity	96	<b>0.118</b>	<b>0.210</b>	0.125	0.217
	192	<b>0.138</b>	<b>0.229</b>	0.144	0.235
	336	<b>0.151</b>	<b>0.244</b>	0.160	0.252
	720	<b>0.173</b>	<b>0.266</b>	0.196	0.283
	Avg.	<b>0.145</b>	<b>0.237</b>	0.156	0.247
Traffic	96	<b>0.335</b>	<b>0.226</b>	0.359	0.241
	192	<b>0.356</b>	<b>0.239</b>	0.377	0.249
	336	<b>0.366</b>	<b>0.246</b>	0.389	0.259
	720	<b>0.402</b>	<b>0.267</b>	0.426	0.284
	Avg.	<b>0.365</b>	<b>0.245</b>	0.388	0.258

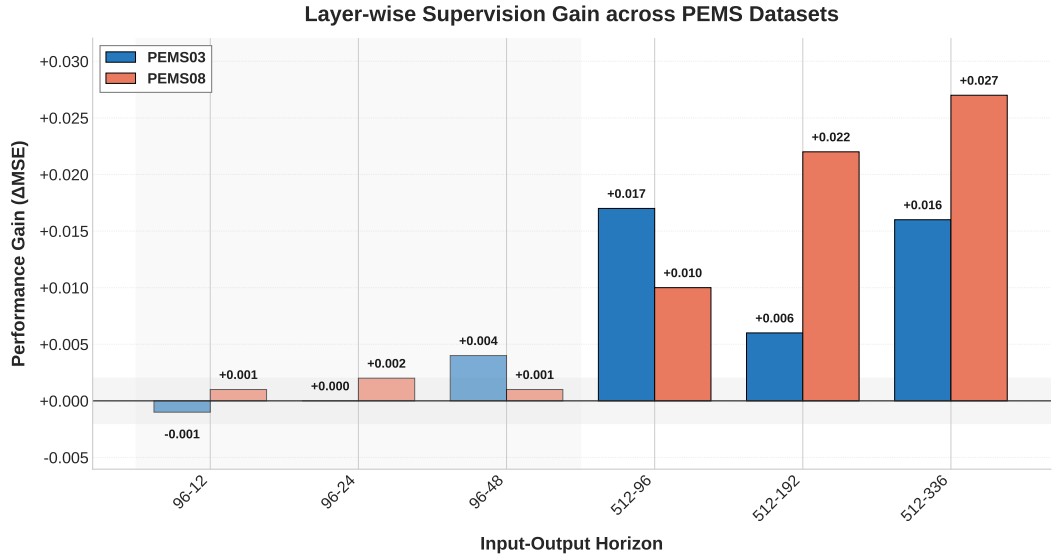
Table 9: Impact of model complexity on performance. **Origin**: The optimal ReNF configuration found via search. **Exchange**: Results when the ReNF variant ( $\alpha$  or  $\beta$ ) is alternated, showing performance degradation when model complexity does not match data characteristics.



(a) Ablation of BDO on M4 Datasets.



(b) Ablation of BDO on PEMS Datasets.



(c) Variation of the Layerwise Supervision Gain across PEMS Datasets

Figure 13: The ablation of two components of BDO. 'w/o sup' removes the block-wise supervision, and 'w/o con' denotes the ReNF removing the block-wise concatenation (thus losing the function of implicit forecast combination). We select TimeMixer Wang et al. (2024b) and TimeMixer++ Wang et al. (2025) as the baseline for M4 and PEMS, respectively. (c) We record the variation of performance gain of block-wise supervision across different forecasting tasks. The advantage of block-wise supervision becomes clearly more significant in the setting of long-term forecasting.

Variants		ReNF		ReNF	
		origin		w/o EMA	
Metric		MSE	MAE	MSE	MAE
ETTh1	96	0.350	0.383	0.357	0.387
	192	0.385	0.408	0.407	0.421
	336	0.405	0.425	0.426	0.435
	720	0.422	0.449	0.447	0.467
	Avg.	0.391	0.416	0.409	0.428
ETTh2	96	0.261	0.329	0.265	0.329
	192	0.320	0.370	0.336	0.375
	336	0.346	0.394	0.397	0.418
	720	0.381	0.423	0.421	0.441
	Avg.	0.327	0.379	0.355	0.391
ETTh1	96	0.270	0.325	0.303	0.347
	192	0.310	0.352	0.341	0.371
	336	0.343	0.373	0.362	0.386
	720	0.401	0.406	0.425	0.420
	Avg.	0.331	0.364	0.358	0.381
ETTh2	96	0.157	0.241	0.162	0.246
	192	0.212	0.279	0.221	0.285
	336	0.262	0.315	0.272	0.322
	720	0.341	0.368	0.352	0.374
	Avg.	0.243	0.301	0.252	0.307

Variants		ReNF		ReNF	
		origin		w/o EMA	
Metric		MSE	MAE	MSE	MAE
Weather	96	0.138	0.180	0.139	0.182
	192	0.181	0.224	0.184	0.227
	336	0.231	0.266	0.232	0.266
	720	0.304	0.318	0.308	0.320
	Avg.	0.214	0.247	0.216	0.249
Electricity	96	0.118	0.210	0.124	0.218
	192	0.138	0.229	0.145	0.239
	336	0.151	0.244	0.156	0.252
	720	0.173	0.266	0.182	0.277
	Avg.	0.145	0.237	0.152	0.247
Traffic	96	0.335	0.226	0.341	0.237
	192	0.356	0.239	0.363	0.249
	336	0.366	0.246	0.373	0.256
	720	0.402	0.267	0.411	0.278
	Avg.	0.365	0.245	0.372	0.255
Solar	96	0.157	0.202	0.177	0.232
	192	0.174	0.210	0.193	0.234
	336	0.180	0.219	0.195	0.239
	720	0.190	0.225	0.199	0.242
	Avg.	0.176	0.214	0.191	0.237

Table 10: Full numerical results on the effect of EMA smoothing.

Variants	ETTh1					ETTh2					Electricity					
	96	192	336	720	Avg.	96	192	336	720	Avg.	96	192	336	720	Avg.	
ReNF	MSE	0.350	0.385	0.405	0.422	0.391	0.261	0.320	0.346	0.381	0.327	0.118	0.138	0.151	0.173	0.145
	MAE	0.383	0.408	0.425	0.449	0.416	0.329	0.370	0.394	0.423	0.379	0.210	0.229	0.244	0.266	0.237
ReNF w/o pre-drop	MSE	0.352	0.385	0.406	0.428	0.393	0.260	0.321	0.348	0.383	0.328	0.119	0.138	0.150	0.175	0.146
	MAE	0.386	0.410	0.429	0.454	0.420	0.329	0.370	0.396	0.425	0.380	0.210	0.229	0.243	0.267	0.237

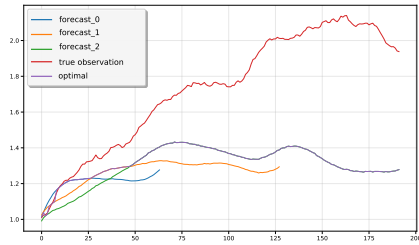
Table 11: Effects of pre-drop.

Model	ReNF		TimeBridge		Confidence Interval
	MSE	MAE	MSE	MAE	
ETTh1	0.391 ± 0.000	0.417 ± 0.000	0.399 ± 0.009	0.424 ± 0.008	99%
ETTh2	0.327 ± 0.000	0.380 ± 0.000	0.343 ± 0.018	0.383 ± 0.014	99%
Weather	0.214 ± 0.000	0.247 ± 0.000	0.219 ± 0.006	0.250 ± 0.003	99%
Solar	0.177 ± 0.000	0.215 ± 0.000	0.182 ± 0.003	0.219 ± 0.003	99%

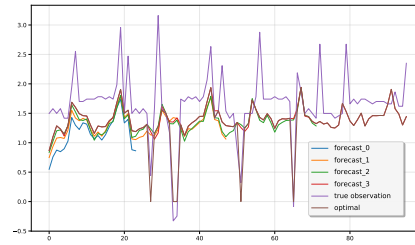
Table 12: Standard deviation and statistical tests for ReNF and TimeBridge on ETTh1, ETTh2, Weather, and Solar datasets. The results are based on the average performance across four prediction lengths from five runs with different random seeds.

## G VISUALIZATION OF PREDICTION

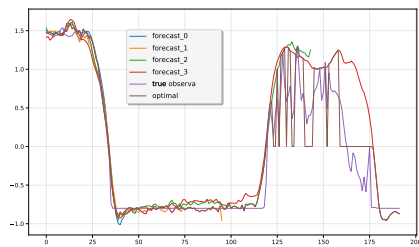
In the following, we present the visualizations of multivariate long-term time series forecasting using ReNF. The predicted variable in each figure is randomly selected.



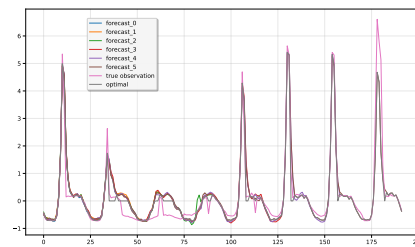
(a) 192-prediction on the weather dataset



(b) 192-prediction on the Electricity dataset

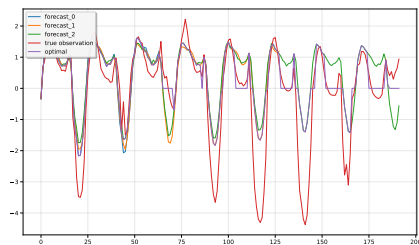


(c) 192-prediction on the Solar dataset

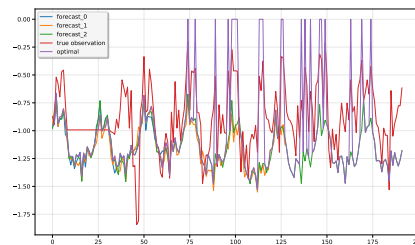


(d) 192-prediction on the Traffic dataset

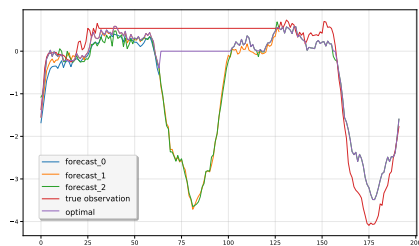
Figure 14: Visualization of forecasting results of ReNF. The figure shows multiple outputs of ReNF in different layers, along with the result of applying optimal post-combination.



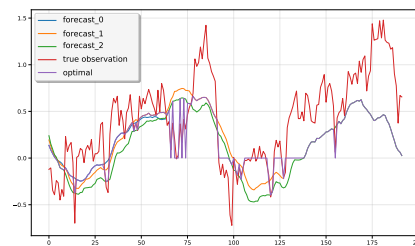
(a) 192-prediction on the ETTh1 dataset



(b) 192-prediction on the ETTh2 dataset



(c) 192-prediction on the ETTm1 dataset



(d) 192-prediction on the ETTm2 dataset

Figure 15: Visualization of forecasting results of ReNF. The figure shows multiple outputs of ReNF in different layers, along with the result of applying optimal post-combination.

## H LIMITATION AND FURTHER DISCUSSION

The Variance Reduction Hypothesis (VRH) presented in this paper is foundational but preliminary. While it provides the core intuition for the multiple forecasting design, a more rigorous and in-depth exploration of its theoretical properties could inspire new and promising research directions. For instance, deriving a bound beyond the independent forecasts would better connect to our proposal, identifying more intricate improvements to the current paradigm.

Specifically, under the paradigm of MNFP, the role of Neural Network (NN) in this area becomes transparent. First and perhaps most importantly, we should leverage NN's capability to create a powerful post-combination function. While our BDO paradigm is effective, the current recursive strategy for combining sub-forecasts is not fully optimal. This is evident from the performance gap between our final forecast and the theoretical empirical bound as the number of stages increases. The core is that while BDO has created the skeleton of sequential causality at the level of network structure, methods for explicitly enforcing the specific causality in this paradigm are required. Developing more intricate methods to better leverage the full set of sub-forecasts could lead to substantial accuracy gains.

Second, we are consistently supposed to build more powerful Neural Forecasting Machines (NFM) to approximate the expected distributions of future data, thereby reducing the bias  $b$  in the MNFP B.1. Therefore, a comprehensive study is needed to verify the effects of our proposed techniques when applied to other advanced model architectures beyond MLPs.

Finally, although we evaluate the effectiveness on diverse short-term forecast benchmarks, this work develops the BDO paradigm specifically for the LTSF setting. A key open question is how this paradigm can be better adapted for diverse forecasting tasks with short length, which could ultimately lead to a more unified framework for time series forecasting.